Biochar

ORIGINAL RESEARCH

Open Access

The dissolved organic matter from the co-decomposition of Chinese milk vetch and rice straw induces the strengthening of Cd remediation by Fe-modified biochar

Ting Liang[1,2†], Guopeng Zhou[3†], Danna Chang[1], Zhengbo Ma[1], Songjuan Gao[4], Jun Nie[5], Yulin Liao[5], Yanhong Lu[5], Hongli Fan[1], Chunqin Zou[2*] and Weidong Cao[1*]

Abstract

Fe-modified biochar (FB) and co-using Chinese milk vetch and rice straw (MR) are two effective ways for mitigating the cadmium (Cd) contamination in paddy fields in southern China. Nevertheless, the effects of FB combined with MR on Cd passivation mechanism remain unclear. In the current study, the strengthening effects of FB induced by MR were found and the mechanisms of the extracted dissolved organic matter (DOM) from the co-decomposition of MR on Cd alleviation were investigated through pot experiment and adsorption experiment. Pot experiment demonstrated that co-incorporating FB and MR decreased available Cd by 23.1% and increased iron plaque concentration by 11.8%, resulting in a 34.7% reduction in Cd concentrations in brown rice compared with addition of FB. Furthermore, co-using FB and MR improved available nutrients in the soil. The molecular characteristics of DOM derived from the decomposition of MR (DOM-MR) were analyzed by fluorescence excitation emission matrix spectroscopy-parallel factor analysis (EEM-PARAFAC) and Fourier transform-ion cyclotron resonance mass spectrometry (FT-ICR MS). Results showed that lignin/carboxylic-rich alicyclic molecules and protein/amino sugar were the main compounds, potentially involved in the Cd binding. Adsorption experiments revealed that the addition of DOM-MR improved the functional groups, specific surface area, and negative charges of FB, inducing the strengthening of both physisorption and chemisorption of Cd(II). The maximum adsorption capacity of Fe-modified biochar after adding DOM-MR was 634 mg g^{-1}, 1.30 times that without the addition of DOM-MR. This study suggested that co-incorporating MR, and FB could serve as an innovative practice for simultaneous Cd remediation and soil fertilization in Cd-polluted paddy fields. It also provided valuable insights and basis that DOM-MR could optimize the performances of Fe-modified biochar and enhance its potential for Cd immobilization.

Handling editor: Lukáš Trakal

† Ting Liang and Guopeng Zhou These authors contributed equally to this work.

*Correspondence:
Chunqin Zou
zcq0206@cau.edu.cn
Weidong Cao
caoweidong@caas.cn
Full list of author information is available at the end of the article

Highlights

- Chinese milk vetch and rice straw strengthened the Cd remediation by biochar.
- Soil DOM was the key influencing factor on soil Cd immobilization.
- DOM optimized the properties of biochar and produced richer functional groups.
- The combination of DOM and biochar had a higher specific surface area than biochar alone.
- DOM strengthened the physisorption and chemisorption capacities of Cd(II) on biochar.

Keywords Cd(II), Fe-modified biochar, DOM, FT-ICR MS, EEM-PARAFAC, Acidic functional groups

Graphical Abstract

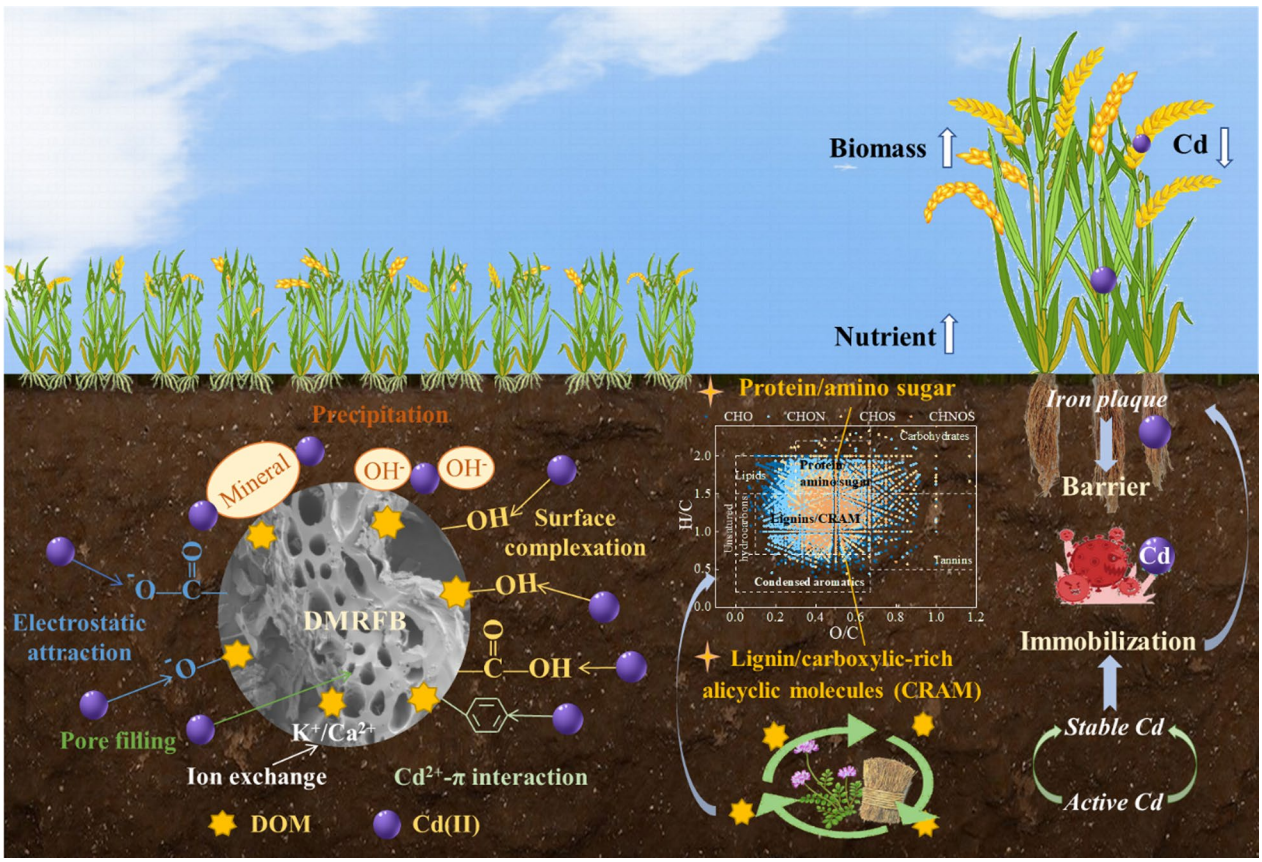

1 Introduction

Cadmium (Cd) is among the serious health risks to humans through the food chain (Wang et al. 2019; Zou et al. 2021). Various soil Cd amendments have been developed for soil Cd passivation over the last years, of which, biochar is the promising material for in-situ passivation methods with various advantages (Arabi et al. 2021; Ok et al. 2020; Palansooriya et al. 2020). Former study has verified the function of biochar to mitigate Cd contamination in water and soil through mechanisms such as adsorption, complexation, and precipitation (Abbas et al. 2017; Yin et al. 2016). Nevertheless, due to the limited stabilization performance of pristine biochar on heavy metals (Shaheen et al. 2022), modified or functionalized biochar is gradually emerging as the novel amendment with outstanding immobilization effect on Cd (Qu et al. 2022a; Shi et al. 2022). Fe-modified biochar (FB) could enhance the sorption sites for Cd due to its rich mesoporous structure and abundant functional groups (Irshad et al. 2022; Zhu et al. 2020). At present, FB

is widely applied in paddy fields and exhibited the strong potential on inhibiting Cd availability (Wan et al. 2020).

Chinese milk vetch (MV) is a winter-growing legume green manure that can balance the soil fertility, enhance rice productivity, and improve environmental quality (Gao et al. 2023). Previous studies revealed that co-incorporating MV and rice straw (RS) played a more remarkable role in reducing Cd availability through promoting the conversion of Cd fractions and the increase of iron plaque (IP), leading to the reduction of Cd content in rice (Zhang et al. 2020a, b). However, the effect is limited, for which the team's recent field experiment was optimized and found that the joint use of MV, RS, and biochar could enhance the reduction of available Cd (Liang et al. 2022). Nevertheless, the explanation for the enhancement mechanism and the role played by MV and RS is unclear and therefore needs to be demonstrated by pot experiments and batch adsorption experiments.

Dissolved organic matter (DOM) is complex, containing components of different molecular weights, and its effect on heavy metals is multifaceted (Min et al. 2021). Previous study discovered that planting perennial green manure ryegrass and straw mulch in orchards improved soil DOM content and composition (Zhang et al. 2019a, b, c). And the DOM obtained from organic material is rich in functional groups, which might complex with heavy metals, thus affecting their morphological structure, mobility, and bioavailability (Plaza et al. 2006). Researchers found that DOM from rice straw promoted iron oxide particle agglomeration and precipitation, immobilizing Cr(III) and enhancing its removal, with carboxyl groups being pivotal (Xia et al. 2022). However, some studies highlighted the contrary effects of DOM, i.e., DOM released from fresh organic material can activate soil Cd due to the high chemical activity of DOM (Xie et al. 2019). These contradictory findings provide challenges and innovative points for this study. Abundant DOM is inevitably released in the field after the decomposition of MV and RS (Zhou et al. 2020a, b, c), which in turn affects the content and composition of soil DOM and might be involved in the speciation transformation of Cd. However, the effect of DOM extracted after the decomposition of MV and RS on biochar passivation for Cd remediation is unclear and needs to be clarified.

Advancing understanding of the synergistic effects of DOM from the decomposition of MV and RS on Cd remediation by FB will help address the relevant knowledge gaps. Herein, the pot experiment was performed involving the effects of incorporation of MV, RS, FB on Cd mitigation. Batch adsorption experiments combined with spectral technologies (XPS, XRD, EEM-PARAFAC, etc.) and high -resolution mass spectrometry (FT-ICR MS) were conducted to analyze the adsorption characteristics, mechanisms of combined treatment, and molecular features of DOM. The study aimed to accomplish the following principal objectives: (1) to explore the effects of FB by MV and RS and the key influencing factors on soil Cd immobilization by co-utilizing MV, RS, and FB in soil-rice system; (2) to determine the impacts of DOM extracted after the decomposition of MV and RS on the properties of FB and Cd(II) adsorption behaviors; (3) to clarify the molecular composition and diversity of DOM; (4) to reveal the Cd(II) adsorption mechanisms by FB regulated by the DOM. We hypothesized that co-incorporating MV and RS could strengthen the soil Cd immobilization ability of FB, and the DOM from MV and RS could optimize the properties of FB and improve the Cd(II) adsorption performance of FB through multiple mechanisms such as precipitation, complexation, and pore filling.

2 Materials and methods

2.1 Preparation of studied soil and materials

The Cd-polluted soil was collected from 0–20 cm depth in the farmland in Heshan, Yiyang City, Hunan Province, China. The soil type is classified as an Entisol Fluvent derived from river alluvium (USDA soil taxonomy). The 10-mesh natural air-dried soil was used in this experiment. Residues and stones in soil were removed. RS used for the experiment was collected from the soil sampling site. The synthesis of FB was prepared based on a previously published procedure (Liang et al. 2022). After a selection of comparative tests, FB with high Cd(II) adsorption capacity was selected for the experiment (Additional file 1: Fig. S1).

2.2 Pot experiment

2.2.1 Experimental design

The pot experiment was carried out from October 2021 to July 2022 in Changsha City, Hunan Province, China. Six amendment treatments were employed: untreated paddy soil (CK-S), MV amendment (MV-S), RS amendment (RS-S), MV and RS mixture amendment (MR-S), Fe-modified biochar (FB-S), and Fe-modified biochar plus MV and RS (MRFB-S). Each treatment was replicated four times. The specific operation is as follows: each plastic basin contained 10 kg soil and MV was sown at a seeding rate of 30 seeds per pot in the treatments containing MV in mid-October 2021. No fertilizers were applied during the MV growth. MV was harvested at the blooming stage (early April 2022). The harvested fresh MV plants were cut into about 1–2 cm pieces and ploughed in situ into the soil together with dry RS and FB 15 d before the transplantation of rice (Zhou et al. 2020b). The dosages of MV, RS, and FB referred to the literature (Liang et al. 2022; Zhou et al. 2020b) (Additional

file 1: Table S1). The chemical fertilizers before rice planting were incorporated into the soil with 0.02% N (Urea), 0.01% P_2O_5 (KH_2PO_4), and 0.02% K_2O (KCl). Fifteen rice seedlings (20 days old) were transplanted in each pot in mid-April 2022 and harvested in late-July 2022. The rice was completely flooded throughout the whole growth period. The basic physicochemical properties of studied soil are shown in Additional file 1: Table S2. The rice seeds (Zhongzao No.39) were used in the pot trials and "Xiangzi No.1" is the MV variety.

2.2.2 Physiochemical analysis

The available Cd (Avail-Cd) was extracted with $CaCl_2$ solution. Cd fraction was measured by previous report (Sutherland and Tack 2002). Basic physical and chemical indicators of soils containing pH, TN, SOC, AP, and AK were analyzed as described by previous study (Bao 2000). Fe^{2+} was analyzed via the o-phenanthroline colorimetric method (Lu 2000). Soil DOM was extracted using ultrapure water (soil: water = 1:5 w/v) and investigated via Multi N/C2100 TOC/N analyzer (Analytik Jena, Germany). The specific extraction and determination methods for iron-plaque are in the Supplementary Material (Method S1). DCB-Fe and DCB-Cd represented Fe and Cd in IP extracted with dithionite-citrate-bicarbonate (DCB) solution, respectively.

The analytical quality and accuracy of the experimental data were ensured using standard materials GBW10014 (GSS-4a) (soil) and GBW10045a (GSB-23a) (rice) for quality control.

2.3 DOM extraction

To explore how the DOM generated from the decomposition of MR affects the Cd(II) adsorption by Fe-modified biochar, DOM extraction experiment was conducted. Decomposition of organic material and DOM extraction were conducted according to the previous method (Hunt and Ohno 2007). Briefly, 190 g of quartz sand, 15 g of MV, 4 g of RS, 220 mL of ultrapure water, and 10 mL of fresh soil inoculum were added to the glass bottle, mixed, and incubated in an incubator at 298 K (MR). The soil inoculum was prepared at a 1:10 ratio of paddy soil to deionized water (w/v). Further details of preparation are shown in supplemental material (Additional file 1: Method S2). CK was added with 100 g of quartz sand and 5 ml of soil inoculum. The MV and RS were incubated with ultrapure water (w/v = 1/10 and 1/20, respectively). The other steps were carried out the same as above. The lost water during incubation was replenished by weighing. Given that the decomposition rate of MV and RS is fast in the early stage and rapid in the later stage (Zhou et al. 2020a), we set up the intensive sampling in the early stages and sparse sampling in the later stages. On days 1, 5, 7, 10, 15, 30, 60, 90, and 120 of decomposition, the samples were shaken continuously for 24 h, centrifuged, and filtered through a 0.45-μm membrane. At last, the extracted filtrate was DOM, which was used for the next experiment. The extracted DOM of CK, MV, RS, and MR were marked as DOM-CK, DOM-MV, DOM-RS, and DOM-MR, respectively.

2.4 Batch adsorption experiments

$Cd(NO_3)_2{\cdot}4H_2O$ was used to prepare the Cd(II) solution for adsorption experiments. The background electrolyte was $NaNO_3$ solution (0.01 mol L^{-1}). Four treatments of different DOM addition were designed: addition of DOM-CK (DCK), addition of DOM-MV (DMV), addition of DOM-RS (DRS), addition of DOM-MR (DMR). One milliliter of DOM solution extracted above (different extraction days) was added into solution contained Cd (35 ml, 200 mg L^{-1}), mixed, shaken (298 K, 180 rpm) for 24 h, and filtered. Finally, the filtrate was employed for analyzing the equilibrium concentration of Cd(II) by ICP-OES. The preliminary result showed that Cd(II) equilibrium concentration was lowest in DMR treatment, indicating that DMR had a stronger Cd(II) adsorption capacity (Additional file 1: Fig. S2). Thus, DOM-MR was used for the later adsorption experiments. Three treatments were set in later adsorption experiments: DCK, FB without DOM addition (FB), and FB with addition of DOM-MR (DMRFB). In DMRFB treatment, 0.01 g of FB material and 1 ml of DOM-MR solution (different extraction days) were added into Cd solution. FB treatment was treated with 0.01 g of FB material. Other steps were conducted as above.

Adsorption kinetics was used to study the time required for adsorption equilibrium. Isothermal adsorption was employed to evaluate the adsorption performance and possible adsorption mechanisms of biochar. In the adsorption kinetics experiments, 0.01 g adsorbent samples were dispersed in a 35 mL Cd(II) solution (200 mg L^{-1}) and shaken, 1 ml DOM-MR solution was added into the solution in DMR and DMRFB treatments. Then, at different time intervals, the samples were centrifugated and filtered through 0.45-μm filter for measurements. Adsorption isotherm experiments for determining the Cd(II) adsorption capacities and isothermal behaviors of biochar were performed in 5, 10, 20, 50, 100, 200, 500, and 1000 mg L^{-1} in solution system. Other steps were the same as above. After last experiment, 10 mg of Cd-loaded FB and DMRFB was washed and added into the $NaNO_3$ system (0.01 mol L^{-1}) for desorption experiment. Then the centrifuge tubes were shaken, filtered, measured to attain the desorption capacity.

Adsorption under different pH and temperature conditions was conducted to assess the adsorption capacity

under various conditions. The influence of pH on Cd(II) adsorption by the biochar was examined within the initial pH range of 3 to 8. The pH of each Cd(II) solution was adjusted using either 0.1 M HCl or 0.1 M NaOH. Each solution containing the adsorbate (35 mL) and an initial Cd(II) concentration of 200 mg L^{-1} was introduced into a 50 mL vial. Additionally, 0.01 g of the adsorbent was added to FB and DMRFB treatments, and 1 ml DOM-MR solution was added into the solution in DMR and DMRFB treatments. Other reaction conditions were as above. For thermodynamic experiments, the reaction temperatures were set at 288 K, 298 K, 308 K, and 318 K. The remaining steps were the same as described above.

2.5 Fluorescence quenching titration and sample analysis

2.5.1 Quenching titration

Before the quenching titration experiment, the DOC concentration of DOM-MR was diluted to less than 10 mg L^{-1} to minimize the influence of inner-filter effects. The metal titration was carried out by adding $Cd(NO_3)_2{\cdot}4H_2O$ titrant (1000 mg L^{-1}) into 25 mL of DOM solution in a 50 mL brown sealed bottle, generating a series of Cd(II) samples with concentrations ranging from 0 to 200 μmol L^{-1} (0, 5, 10, 20, 50, 100, and 200 μmol L^{-1}). In the DMR treatment group, 1 mL of DOM-MR solution and Cd(II) solution at various concentrations were added. In the FB treatment group, 0.01 g of FB and 0 μmol L^{-1} Cd(II) were used. The DMRFB treatment group included 0.01 g of FB, and 0 μmol L^{-1} Cd(II), and 1 mL of DOM-MR solution. During the titration process, 0.1 mol L^{-1} NaOH or HNO_3 solution was used for pH adjustment to maintain the pH at 6.0, and the addition of the metal titrant did not exceed 50 μL to avoid concentration effects. All titration solutions were shaken in a dark environment at 298 K for 24 h to ensure complexation equilibrium (Wu et al. 2011). Subsequently, the solutions were filtered and the filtrate was analyzed using fluorescence EEM spectroscopy. Moreover, the solution without Cd (0 μmol L^{-1} Cd) was subjected to desalination treatment (Qi et al. 2021), and the molecular composition was determined using ultra-high-resolution Fourier transform ion cyclotron resonance mass spectrometry (FT-ICR MS) (Solarix 2XR, Bruker, Germany) equipped with an electrospray ionization source (ESI) in the negative ion mode.

2.5.2 EEM-PARAFAC and FT-ICR MS analysis

The fluorescence spectra of the aforementioned samples were measured using a fluorescence spectrophotometer (F-7000, Hitachi, Japan). The method was as follows: ultrapure water was used as a blank, with excitation (Ex) wavelengths ranging from 200 to 500 nm at 5 nm intervals, and emission (Em) wavelengths ranging from 250 to 550 nm at 2 nm intervals. The scanning rate was set at 2400 nm min^{-1}. The slit widths for both emission and excitation were set to 5 nm. PARAFAC analysis was performed using the DOMFluor toolbox (http://www.models.life.ku.dk/) in MATLAB R2022 (MathWorks, Natick, MA) (Stedmon and Bro 2008), with models incorporating non-negativity constraints and ranging from two to seven components. The number of fluorescent components was identified through a combination of residual analysis, split-half testing, and visual inspection. To validate the fluorescence components extracted by PARAFAC, the Ex and Em values of the fluorescent components were uploaded to the OpenFluor online database (http://www.openfluor.org) for quantitative comparison and confirmation. Molecular formula assignment was conducted using the TRFu algorithm. DOM components were classified into seven categories: protein/amino sugar, lipids, carbohydrates, unsaturated hydrocarbons, tannins, lignin, and condensed aromatics based on their O/C and H/C values. The classification boundaries are presented in Additional file 1: Table S3 (Huang et al. 2022; Liu et al. 2023). The classification criteria for carboxylic-rich alicyclic molecules (CRAM) are DBE/C = 0.30 ~ 0.68, DBE/H = 0.20 ~ 0.95, and DBE/O = 0.77 ~ 1.75 (Hertkorn et al. 2006).

2.6 Characterization of samples

The freeze-dried DOM of MR (DMR), FB material, and DMR + FB (DMRFB) samples were used for characterization (SEM–EDS, XRD, FT-IR, XPS). The morphological structure, distribution of key elements, functional groups, the concentrations of acidic functional groups, elemental analysis, zeta potentials, specific surface areas (S_{BET}), pore-size distributions, and crystal structure of FB and DMRFB were measured as described in Additional file 1: Method S3.

2.7 Statistical analysis

The adsorption capacities and removal efficiencies of Cd(II) by the FB and DMRFB were calculated by the formulas in Additional file 1: Method S4. Isotherms and kinetics data for Cd(II) sorption were fitted using some models as described in Method S4. The formulas for calculating enthalpy change (ΔH), entropy change (ΔS), Gibbs free energy (ΔG), and activation energy (E_a) in thermodynamic analysis are provided in the supplementary materials (Method S4). In order to characterize the overall molecular features of DOM, modified aromaticity index (AI_{mod}), double bond equivalent (DBE), molecular weight (MW), and nominal oxidation state of carbon (NOSC) were calculated in Additional file 1: Table S4 according to the formulas, which are provided in Additional file 1: Method S4.

To investigate the significant differences in various physicochemical parameters between experimental treatments, repeated-measured analysis of variance (ANOVA) and multiple comparisons of LSD at 5% level of probability ($P < 0.05$) was used for normally distributed data. And Friedman test and Mann–Whitney-U-Test were applied for non-normally distributed data (Additional file 1: Table S5).

All figures in this study were made using Origin 2022 software. FT-IR, XRD, and XPS data were analyzed by OPUS 7.5.18 software, jade 6, and XPSPEAK41, respectively.

3 Results and discussion

3.1 Effect of amendments on Cd bioavailability and soil properties in pot experiments

MRFB-S significantly enhanced pH by 0.73 and 0.11 units compared with that in MR-S and FB-S treatments, respectively ($P < 0.05$) (Fig. 1A). The improvement of pH would facilitate the soil Cd immobilization (Yin et al. 2017). DOM is the active component of soil and is inextricably and complexly linked to the activities of Cd. (Feng et al. 2021). In the current study, DOM was the highest in MRFB-S treatment (Additional file 1: Table S6). Compared with CK-S and MR-S, MRFB-S significantly increased DOM by 22.3% and 15.6%, respectively ($P < 0.05$). Furthermore, other chemical properties might indirectly influence the Avail-Cd to a certain extent (Wang et al. 2022a, b, c). Soil AP and AK were the highest in MRFB-S. Compared with FB-S and CK-S, MRFB-S significantly elevated the AK by 88.3% and 97.4%, respectively ($P < 0.05$). Avail-Cd acts as a major role in regulating the Cd uptake by crops (Wu et al. 2020). The present study showed that MRFB-S reduced Avail-Cd concentration by 81.4%, 76.3%, and 23.1%, respectively, compared with CK-S, MR-S, and FB-S, respectively (Fig. 1B). Overall, MRFB-S provided more soil available nutrients for rice growth and more favorable soil environment for limiting Cd mobility.

In addition, the concentrations of different Cd species were arranged from largest to smallest as follows: acid-soluble Cd (Aci-Cd), reducible Cd (Red-Cd), oxidizable Cd (Org-Cd), and residual Cd (Res-Cd) (Fig. 1C). Aci-Cd is the most phytoavailable Cd among the four Cd fractions mentioned above (Matong et al. 2016), consisting with the current results that Aci-Cd was extremely positively related to the Cd in different tissues ($P < 0.01$) (Additional file 1: Fig. S3). In Fig. 1C, MV-S, RS-S, MR-S, FB-S, and MRFB-S treatments reduced the Aci-Cd concentrations by 22.3%, 26.6%, 25.8%, 27.6%, and 32.2%, respectively, and the lowest Aci-Cd concentration was observed in MRFB-S treatment. Org-Cd and Red-Cd did not show significant level in the six treatments ($P > 0.05$). The Cd fractionation reflected the underlying availability and mobility of Cd (Matong et al. 2016). MRFB-S reduced Aci-Cd, increased Res-Cd, and altered the distribution of Cd fractions, confirming previous studies that adding passivated materials can lead to redistribution among different geochemical forms (Yang et al. 2020).

MRFB-S exhibited the highest level of Fe concentration in IP among all treatments and the DCB-Fe concentration was increased by 11.8% compared with FB-S (Fig. 2A). As compared with MR-S, MRFB-S elevated the DCB-Fe and DCB-Cd concentration by 37.2% and 35.9%, respectively ($P < 0.05$). Fe^{2+} was a main factor in the formation of IP (Antoniadis et al. 2017). Iron modification of biochar generally helped in the formation of IP on the roots of rice plants. Research has found that Nano-Fe_3O_4-modified biochar promoted the formation of IP on root surfaces and reduced the toxicity of Cd to rice roots (Zhang et al. 2020a, b). In this study, MRFB-S showed the highest Fe^{2+} concentration among all treatments and significantly elevated the Fe^{2+} levels by 82.6% and 65.9% compared with CK-S

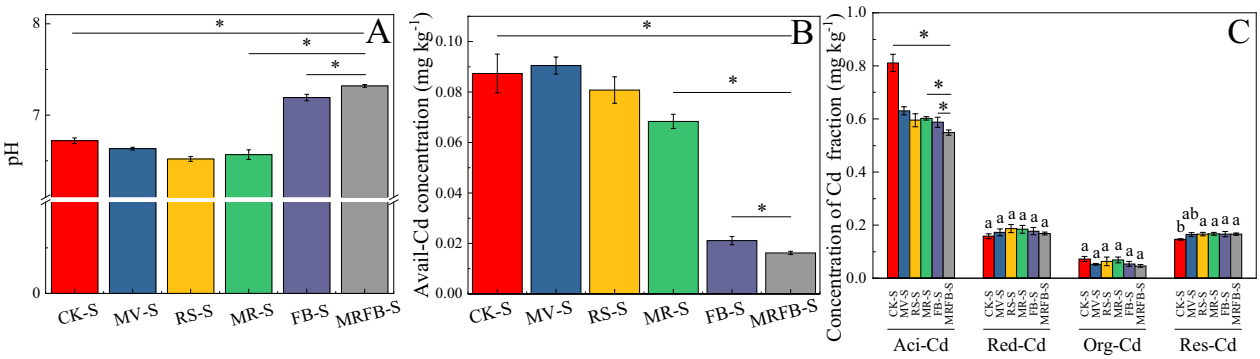

Fig. 1 pH value, Avail-Cd concentration, and Cd fraction under different treatments. ($P < 0.05$; *, $P < 0.01$; **, $P < 0.001$; ***, the same below. **A** pH; **B** Avail-Cd concentration; **C** Cd fraction)

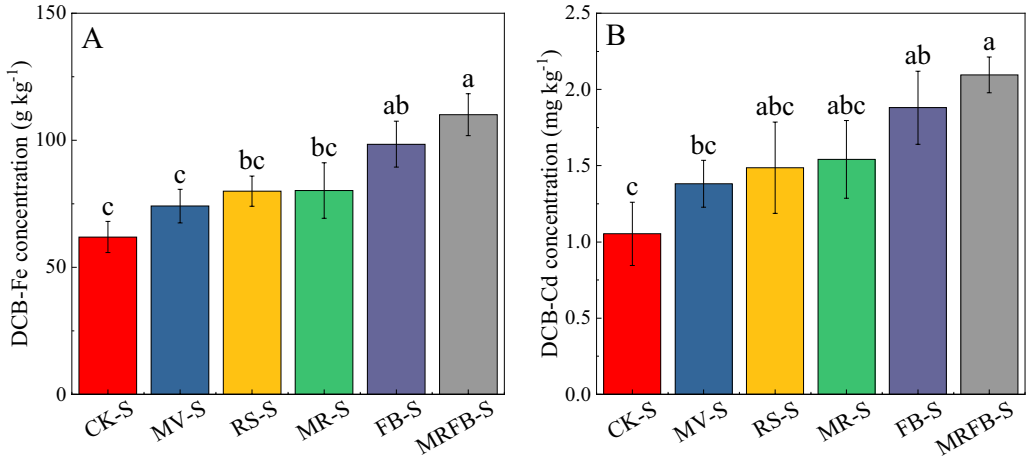

Fig. 2 Concentrations of DCB extractable Cd and Fe in iron plaque

and MR-S treatments ($P < 0.05$) (Additional file 1: Fig. S4). In the present study, DCB-Fe was obviously positively influenced by soil Fe^{2+} ($P < 0.001$) (Additional file 1: Fig. S3), indicating that Fe^{2+} contributed to the formation of IP. Besides Fe^{2+}, pH, soil redox (Eh), soil microorganisms, and radial oxygen loss (ROL) also regulated the IP formation (Zhang et al. 2019a, b, c; Zhang et al. 2018). Numerous studies observed that the adding of biochar and green manure could increase soil pH and reduce Eh, thereby facilitating IP formation on roots (Irshad et al. 2022). This finding aligns with the results obtained in our study indicating that obvious positive correlations appeared between pH and DCB-Fe as well as DCB-Cd ($P < 0.01$). Another finding was that the increasing rice biomass in MRFB-S may help to increase root activity and thus increase ROL (Additional file 1: Fig. S5). Some research also evidenced that the addition of MV-S or RS-S could promote greater microbial iron reduction via soil reducing-bacteria (Zheng et al. 2022), and result in a larger increase in soil pH following submergence, thus facilitating the formation of IP.

The Cd levels observed in the different parts of rice plant were ranked as follows: the highest in root, followed by shoot, and the lowest in brown rice (Fig. 3). The root is the primary gateway for Cd to enter the rice from the soil and is the main tissue of Cd accumulation, which is significantly and positively correlated with effective Cd (Additional file 1: Fig. S3). The Cd absorbed by rice roots and transported to the above-ground part was mainly distributed in rice straw, while the proportion of Cd in the rice grain was small, which also reduced the risk of Cd entering the food chain from another perspective (Chen et al. 2021a, b). Compared with CK-S, MR-S, and FB-S treatments, MRFB-S treatment greatly lowered the Cd concentrations of brown rice by 86.2%, 82.5%, and 34.7%, respectively. Among these treatments, Cd level in brown rice treated with MRFB-S did not surpass the

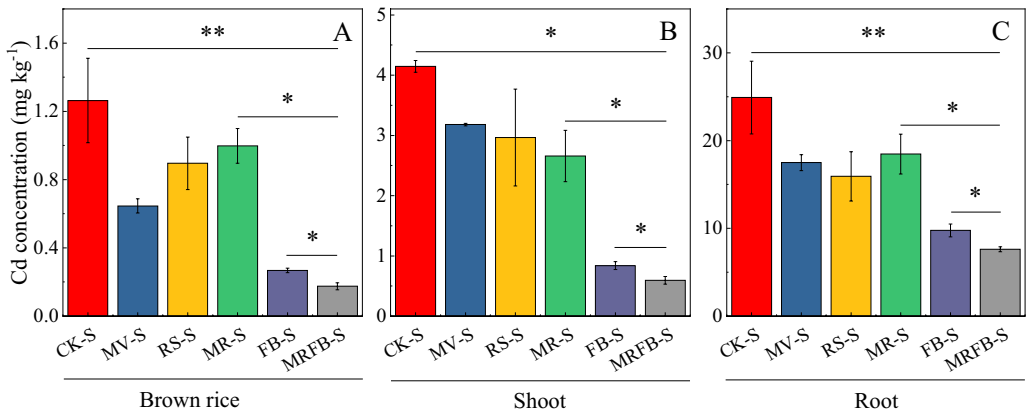

Fig. 3 Cd levels in rice different parts

Cd safety threshold (0.2 mg kg^{-1}). For the shoot and root, MRFB-S also showed the lowest Cd concentration, significantly decreased by 77.7% and 58.8% compared to MR-S, 29.1% and 22.1% compared to FB-S, respectively ($P < 0.05$). Moreover, MRFB-S not only reduced the Cd level in the rice plant, but also greatly improved the biomass of the rice grain and shoot by 71.9% and 58.2%, respectively, compared with CK-S (Additional file 1: Fig. S5). A previous study has found that Fe-modified biochar greatly reduced the Cd level in rice plants, mainly due to the passivation of Cd, the generation of stable Cd complexes, and the dilution effect induced by the increase of crop biomass (Sun et al. 2021). Some researchers also evidenced that co-using milk vetch and rice straw promoted the transformation from active Cd to a steady form (Wang et al. 2022a, b, c). In the present study, MRFB-S greatly reduced the Cd availability and boosted the conversion of the Cd species in soil to more stable residual states, thereby blocking the Cd uptake by the rice plant. Additionally, MRFB-S treatment facilitated the formation of IP, hindering or decreasing the movement of Cd into rice root system, further inhibiting the Cd adsorption by rice (Yin et al. 2017). These findings were favored by the current result that there was a greatly negative correlation between DCB-Fe and total Cd in different tissues of rice plant ($P < 0.001$) (Additional file 1: Fig. S3). Overall, the co-incorporation of MV, RS, and FB was an effective measure that could take into account both soil fertilization and cadmium pollution control.

3.2 Effects of key factors on Cd bioavailability

In addition to the environmental variables (e.g., Cd fraction) directly related to Avail-Cd, there are multiple indirect factors (soil physiochemical properties) affecting the Cd bioavailability. To assess the importance of physiochemical properties on Avail-Cd levels as shown in Additional file 1: Table S6, we performed the random forest regression model (Fig. 4A). Among the soil physiochemical properties, DOM had the highest Inc MSE value, suggesting that DOM played an extremely critical role in regulating the Cd availability. The combination of Cd with DOM has been widely reported to constrict mobility of Cd (Borggaard et al. 2019). In the present study, DOM was negatively associated with Avail-Cd (Additional file 1: Fig. S3), suggesting that higher DOM helped reduce the Cd availability. Nevertheless, researchers found that the DOM from air-dried cotton stalk and farmyard manure reduced the exchangeable Cd due to its more components with low molecular weight, low aromaticity, and high hydrophilicity (Min et al. 2021). We speculated that the composition of DOM generated from fresh samples and decomposition differed. DOM produced from the co-decomposition of milk vetch and rice straw predominantly consisted of high molecular weight compounds, which might contribute to the reduction of Cd activity. pH was another imperative factor and highly negatived related to Avail-Cd (El-Naggar et al. 2022), and this agreed with the results of the current study (Additional file 1: Fig. S3).

Partial least squares path model (PLS–PM) further discerned the relationships and influences of related parameters on brown rice Cd levels (Fig. 4B). Therein, the goodness of fit (GOF) statistic (GOF = 0.796) evaluated the model well. Soil pH was significantly positively correlated with DOM (0.63) ($P < 0.001$) and Fe^{2+} (0.58) ($P < 0.01$). DOM (−0.44) and pH (−0.53) strongly and negatively affected the Avail-Cd ($P < 0.01$), indicating that higher pH and DOM levels favored the reduction of Avail-Cd. The latent variables (IP) represent DCB-Fe and DCB-Cd. Fe^{2+} showed a significant and positive

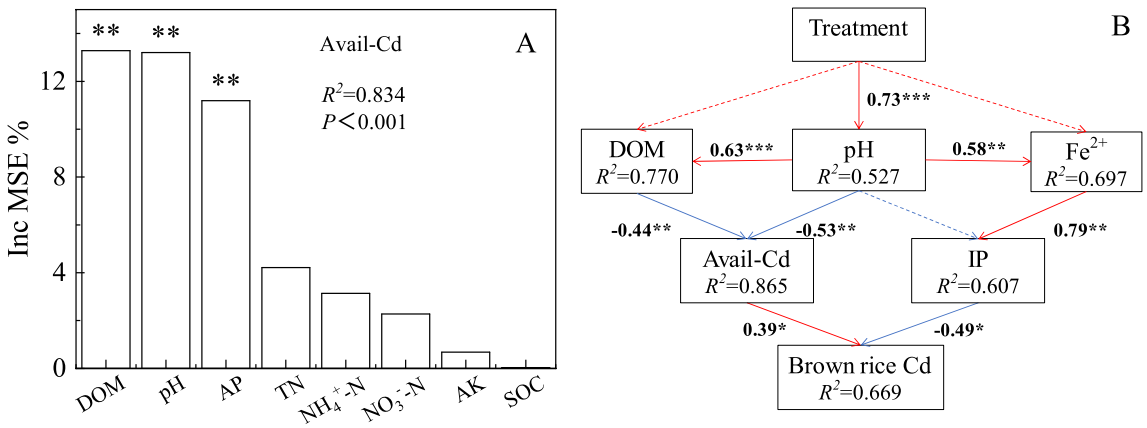

Fig. 4 Random Forest regression model and PLS–PM. Introduction of the parameters are in the supplementary material (**A** Random Forest regression model; **B** PLS–PM)

correlated with IP (0.79) ($P<0.01$). Moreover, Avail-Cd was directly and positively related to brown rice Cd (0.39) ($P<0.05$), suggesting that the decrease in Avail-Cd benefited the mitigation of Cd uptake by brown rice. IP had a negative effect on it (−0.49) ($P<0.05$). This result could be supported by the finding of Zhou et al. (2018), who found that Cd content in IP was significantly or highly significantly correlated with Cd in whole rice plants. In summary, DOM plays a crucial role in regulating the bioavailability of Cd.

3.3 Characterization of DMR, FB, and DMRFB

The SEM graphs and EDS spectra showed the surface morphology and main element composition of FB and DMRFB, both of which had visible loose structure and multi-element characteristics (Additional file 1: Fig. S6). DMRFB exhibited uneven surfaces with more particles and highly porous structure compared with FB. Elemental analysis indicated that DMRFB increased oxygen element concentration by 12.5% relative to FB (Table 1), implying that the presence of DOM generated from MR decomposition increased the abundance of oxygenated functional groups in FB (Lyu et al. 2022a). Unsurprisingly, compared with DMR and FB, DMRFB contained richer functional groups (carboxyl, hydroxyl, carbonyl, and esters) (Additional file 1: Fig. S7A). Moreover, DMRFB had higher oxygen-to-carbon ratio, implying DMRFB was highly aromatic.

The N_2 adsorption–desorption characteristics of FB and DMRFB as well as the volume and size of the pores were analyzed. DMRFB showed larger pore volume and smaller average pore sizes than those of FB, which were more conducive to the pore adsorption for Cd (Table 1). Besides, the curve was a typical IV type with H3 hysteresis loop characteristic of mesoporous materials, according to the IUPAC classification (Additional file 1: Fig. S8C) (Qu et al. 2022a). The above results of BJH analysis and adsorption curve features for DMRFB and FB indicated that mesoporous structures predominated its morphological feature in line with the result of pore-size distributions (Additional file 1: Fig. S8D). Additionally, the S_{BET} is a vital indicator of the sorption ability of adsorbent. The S_{BET} of DMRFB (49.4 $m^2\ g^{-1}$) was significantly higher compared to that of FB (24.9 $m^2\ g^{-1}$) (Table 1), 1.99 times that of FB, indicating that DMRFB has the potential to offer a larger quantity of active adsorption points for Cd(II) (He et al. 2018).

The XRD patterns of DMR, FB, and DMRFB reflected their excellent crystalline nature and contained numerous minerals. In XRD profiles of FB and DMRFB (Additional file 1: Fig. S7E), the peaks at 18.05° and 47.13° belonged to (001) and (102) planes of $Ca(OH)_2$ (JCPDS PDF 81-2040), respectively. Correspondingly, the other diffraction peaks at 29.37°, 43.12°, and 47.45° were assigned to the (104), (202), and (018) planes of $CaCO_3$ (JCPDS PDF 72-1937), respectively. The characteristic peak of all materials at 39.38° represented FeO(OH), and the peaks at 50.70° and 34.08° corresponded to (211) planes of α-FeO(OH) (JCPDS PDF 17-0536) and (200) planes of $FeSO_4$ (JCPDS PDF 12-0068). KCl was found at 28.59°. In XRD profiles of DMR, KCl (JCPDS PDF 75-0296) and $KHCO_3$ (JCPDS PDF 12-0292) were the major phases (Additional file 1: Fig. S7B).

3.4 Cd(II) adsorption performance of FB and DMRFB

3.4.1 Adsorption isotherm and kinetic analysis

At a certain concentration of Cd solution, the Cd(II) equilibrium concentrations observed with DMR and FB treatments were higher than that found in DMRFB treatment. Additionally, as the DOM extraction time prolonged, the influence of DMRFB on Q_e stabilized gradually (Additional file 1: Fig. S9). The linear correlation analysis indicated that Cd(II) equilibrium concentration was negatively correlated with pH (Additional file 1: Fig. S10). It was also found that DMRFB with the lowest Cd(II) equilibrium concentration had a higher pH value than FB, which was more conducive to the acquisition of precipitation (e.g., $Cd(OH)_2$) (Yin et al. 2020). The removal efficiency of DMRFB on Cd(II) reached 93.0% at 120 d, 9.28% higher than FB treatment. Thus, the addition of DOM-MR induced the strengthening of Cd immobilization by FB.

The isotherm results showed that the Langmuir formula could better simulate isothermal data than Freundlich to describe the adsorption process ($R^2=0.942$ versus $R^2=0.869$, Additional file 1: Table S7), i.e., monolayer adsorption mainly involved in adsorption (Liang et al. 2020) (Fig. 5A). The maximum Cd(II)

Table 1 The basic physicochemical properties of biochar

Material	S_{BET}	Average pore diameter	Total volume in pores	Zeta potential	Elemental (%)				
	($m^2\ g^{-1}$)	(nm)	($\times 10^{-3}\ cm^3\ g^{-1}$)	(mV)	C	O	N	H	S
FB	24.9	9.00	55.9	− 2.00	20.5	24.4	0.42	1.85	0.32
DMRFB	49.4	5.00	61.8	− 20.4	22.3	27.4	0.42	1.81	0.21

S_{BET} means specific surface area

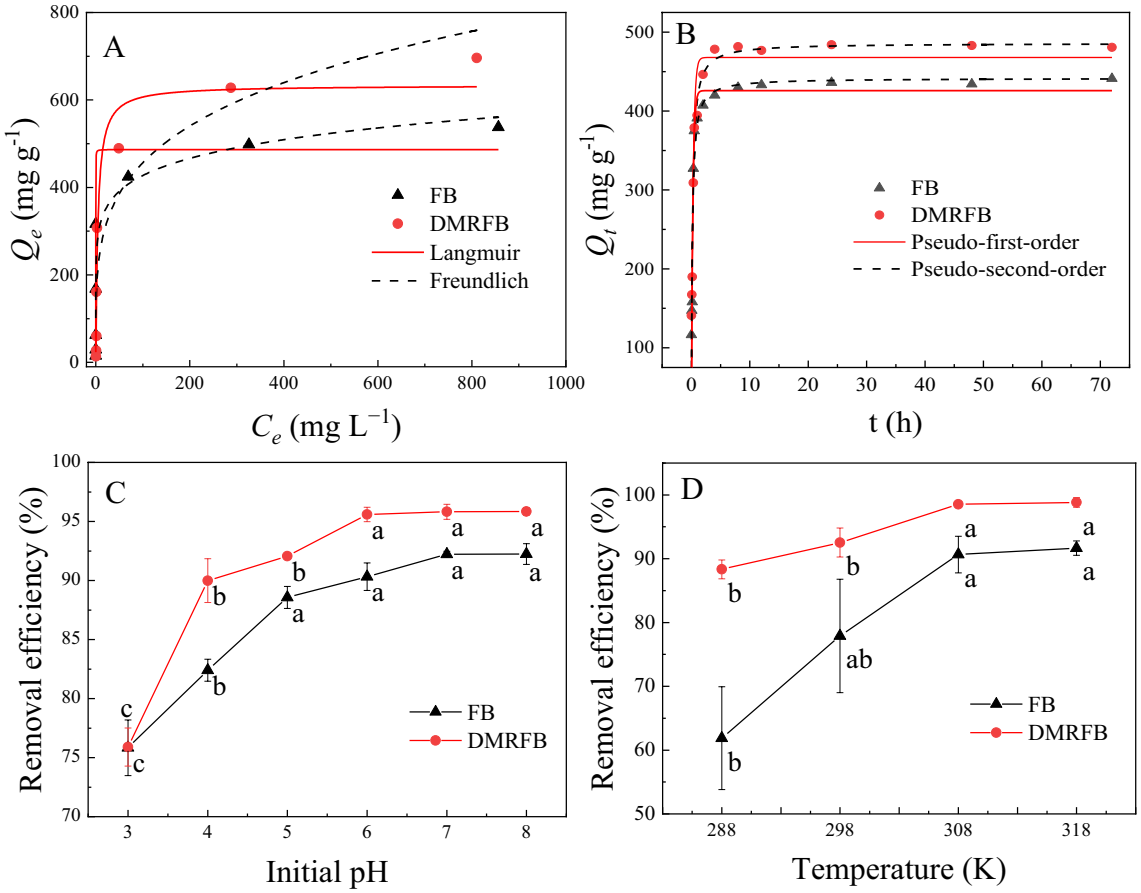

Fig. 5 Isotherm fitting and kinetic fitting results of Cd(II) adsorption (**A** and **B**) and effect of pH and temperature on Cd(II) adsorption (**C** and **D**)

adsorption capacities (Q_m) ranked in the order of DMRFB (634 mg g^{-1}) > FB (487 mg g^{-1}), and the Q_m of DMRFB for Cd(II) was far ahead in many literatures (Additional file 1: Table S8) (Tan et al. 2022; Zhang et al. 2022a, b, c). Moreover, the EDS analysis verified that successful immersion of Cd onto surface of both FB and DMRFB, and the weight ratio of Cd in the Cd-adsorbed materials was ranked as DMRFB > FB after adsorption (Additional file 1: Fig. S8A and B, respectively). The desorption experiment showed that DMRFB had the low desorption efficiencies (Additional file 1: Fig. S11), indicating that Cd(II) was difficult to desorb. Therefore, DMRFB had a strong and stable ability to immobilize Cd(II), effectively mitigating the environmental risks associated with the migration of toxic and hazardous Cd ions.

The adsorption kinetic processes of Cd(II) by FB and DMRFB were similar and the curve was divided into two periods. The adsorption capacity largely increased within the first 0.5 h, after which it remained stable (Additional file 1: Fig. S5B). The swift adsorption phase can likely be ascribed to the rapid intrusion of Cd(II) into the adsorption sites located on the exterior surface of the biochar, potentially by means of physical adsorption (Yin et al. 2020). When the milk vetch decomposes, there are negatively charged humic acid produced at the same time. In current results, the zeta potential of DMRFB was lower than that of FB (Table 1), indicating that DMRFB had more negative charges and thus gained a stronger electrostatic attraction to cations (Cd). During the slow adsorption phase, the adsorption approached saturation due to a large number of Cd(II) covering on the exterior surface, leading to fewer active points available for further adsorption and a levelling off of the adsorption curve (Fig. 5B). Obviously, pseudo-second-order model obtained a better match for Cd(II) adsorption with higher correlation coefficient (0.932 and 0.923) than pseudo-first-order model (0.891 and 0.922), showing that the adsorption reaction was mainly chemisorption of Cd(II) (Zhou et al. 2017). Additionally, DMRFB showed the higher adsorption rate constant (K_2) than FB (Additional file 1: Table S9), indicating that DMRFB achieved a more rapid adsorption of Cd(II). Similarly, DMRFB showed higher measured and predicted Cd(II) adsorption capacity than FB.

3.4.2 Effect of pH and temperature on Cd(II) adsorption

Generally speaking, the initial pH value of the solution will alter the surface charge of the adsorbent in the aqueous solution, thereby impacting the form and adsorption efficiency of metal ions (Yin et al. 2020). In this study, under low pH conditions, both FB and DMRFB exhibited low removal efficiencies for Cd(II) (Fig. 5C), which may be attributed to the highly protonated surfaces of FB and DMRFB, as well as the presence of oxygen-containing groups carrying positive or neutral charges, resulting in strong electrostatic repulsion towards Cd(II) (Sun et al. 2023). As the solution's pH value increased, the positive charge on the surfaces of FB and DMRFB gradually decreased. When the pH value exceeded 7, the removal rate of Cd(II) of DMRFB reached its peak (up to 95.8%). It was speculated that a significant amount of $Cd(OH)_2$ precipitate might have formed (Li et al. 2017). Furthermore, DMRFB consistently exhibited higher removal efficiency for Cd(II) compared to FB, which could be attributed to the relatively higher negative charge of DMRFB itself.

Thermodynamic studies were conducted for the adsorption of Cd(II) on FB and DMRFB at temperatures of 288, 298, 308, and 318 K, and the thermodynamic parameters are shown in Additional file 1: Table S10. With increasing reaction temperature, the Cd(II) adsorption capacity of both FB and DMRFB continuously increased, indicating that these adsorbents are more effective in adsorbing Cd(II) at higher temperatures (Zheng et al. 2021). The positive value of ΔH confirmed that the adsorption of Cd(II) on FB and DMRFB was an endothermic process, hence higher temperatures favored the capture of pollutants (Lyu et al. 2022a). Similarly, as the temperature increased, E_a gradually decreased, indicating that less energy was required for the reaction, leading to an increase in the reaction rate (Additional file 1: Table S11). The negative value of ΔG indicated that the adsorption process was feasible and thermodynamically spontaneous, with DMRFB exhibiting a better absolute value of ΔG. Furthermore, the positive value of ΔS suggested an increase in randomness at the solid-solution interface during the removal of Cd (II) by FB and DMRFB.

3.4.3 Insight into the adsorption mechanism

The surface functional groups of FB and DMRFB were observed by FT-IR spectrum (Additional file 1: Fig. S8F). A broad and strong absorption peak appeared in the 3700–3200 cm^{-1} region, corresponding to –OH stretching vibration bond. The –CH band was present at 878 and 710 cm^{-1}, and 1433 cm^{-1} was the functional groups associated with CO_3^{2-} (Liu et al. 2020; Zhao et al. 2020). It is evident from the figure that in the presence of DOM, the peak intensities of these functional groups were significantly enhanced, indicating that DMRFB had a richer variety of functional groups. The other stretching vibration peaks at 1795, 1586, and 1018 cm^{-1} were assigned to carboxyl C=O, aromatic C=C, and alkoxy C–O–C, showing an apparent shift after DMR treatment (Zhang et al. 2022a, b, c). Overall, DOM-MR increased the surface functional groups numbers (–OH, C=O, CO_3^{2-}, C–O–C, C=C, and –CH) of biochar to some extent. In agreement with the result of the concentrations of the acidic functional groups of FB and DMRFB measured by Boehm titration (Boehm 1994), DMRFB had more acidic functional groups than FB (Additional file 1: Table S12). For example, total acidic functional groups and phenolic of DMRFB enhanced by 13.7% and 20.1% than those of FB, which could facilitate the complexation between acidic functional groups and heavy metals (Chen et al. 2021a, b). After Cd(II) adsorption. The peak intensity of DMRFB at 3441^{-1} declined, suggesting the involvement of -OH functional groups in Cd(II) adsorption (Trakal et al. 2016). Similarly, alterations in C=C, CO_3^{2-}, C=O, C–O–C, and –CH functional groups after adsorption pointed towards their vital role in the Cd fixation (Mujtaba Munir et al. 2020). Although the functional groups experienced a shift in position and changed in peak intensity after Cd(II) adsorption, the types and quantity of functional groups did not decrease. This indicated that the adsorption process did not cause substantial damage or loss of functional groups in DMRFB.

For further observation of the chemical composition and valence states of key elements, as well as the changes of functional groups involved in Cd(II) binding, XPS analysis demonstrated the shifts in chemical constituents of FB and DMRFB before and after Cd(II) sorption. The full survey scans results indicated that the surfaces of FB and DMRFB were mainly distributed with C, O, Fe, and Ca, and that the semi-quantitative content of these elements did not undergo significant changes before and after Cd(II) adsorption (Additional file 1: Table S13). These findings further supported the stability of DMRFB after Cd(II) adsorption. However, after Cd(II) adsorption, a new peak (Cd 3d) could be detected (Fig. 6A), implying that numerous Cd ions adsorbed onto DMRFB. Additionally, Cd ions could take away the binding point of Ca ions on the material surface (Lyu et al. 2022b). As presented in Fig. 6A, peak intensity of atomic of the Ca 2p spectrum was decreased after Cd(II) adsorption, indicating that ion exchange might be associated with the Cd binding step (Qiao et al. 2018). The analyses of SEM–EDS, XRD, and XPS indicated that DMRFB had more K ions and Ca ions than FB due to the introduction of DMR, suggesting that DMRFB exhibited superior ion exchange capacity (Fig. 6D, S7, and Additional file 1: Fig. S8B, E). Three different characteristic peaks of O 1 s spectra before

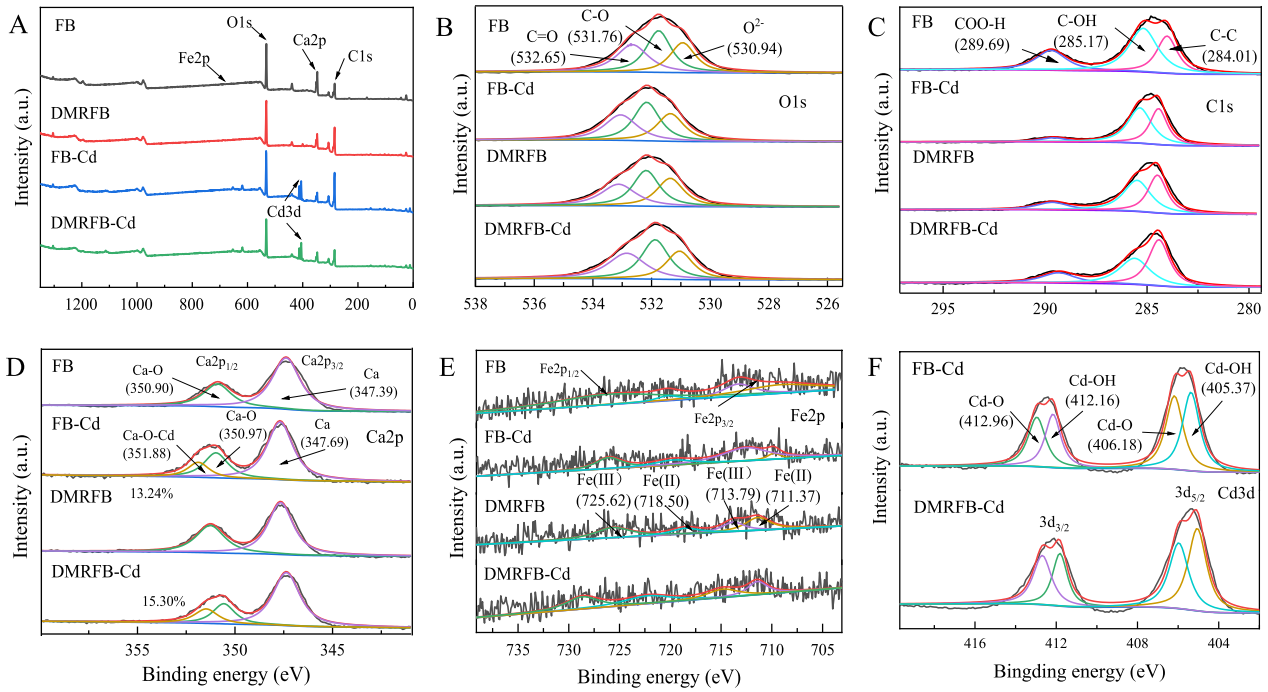

Fig. 6 XPS survey spectra of FB and DMRFB. **A** is XPS survey spectra of the whole. **B**, **C**, **D**, **E**, and **F** are high resolution XPS spectrum of O 1 s, C 1 s, Ca 2p, Fe 2p, and Cd 3d, respectively

the Cd(II) adsorption were found at 531.36, 532.18, and 533.11 eV for DMRFB, consistent with the lattice oxygen (O^{2-}), C–O, and C=O peaks, respectively. Nevertheless, these peaks shifted slightly after Cd binding, revealing that the carboxyl and hydroxyl groups were successfully involved in the adsorption (Wang et al. 2022a, b, c). In the C 1 s spectra, peaks for C–C, COO–H, and C–OH altered post Cd(II) adsorption by FB and DMRFB, corroborating with FTIR results, indicating significant involvement of –COOH and –OH groups in Cd binding (Bolan et al. 2014). As observed from Fig. 6D, a new characteristic peak of Ca2p at 351.88 eV (Ca–O–Cd complex) appeared after the stabilization of Cd (Lyu et al. 2022b), with more complexes formed by DMRFB (15.3%) than FB (13.2%), suggesting that DMRFB displayed stronger adsorption capacity than FB. The Fe 2p spectra peaks in DMRFB appeared at 718.50 and 711.37 eV, attributed to the species of Fe(II) 2p1/2 and Fe(II) 2p3/2, respectively, while peaks at 725.62 and 713.79 eV represented the satellite peaks of Fe(III) 2p1/2 and Fe(III) 2p3/2, respectively. The semi-quantitative analysis revealed that in FB, the Fe(II) content accounted for 34.4%, Fe(III) was 65.6%, while those in DMRFB were 45.5% (Fe(II)) and 54.4% (Fe(III)), respectively. This indicated that DMRFB was more efficient than FB at reducing Fe(III) to Fe(II). In addition, the peaks of Cd 3d explored at 412.69 and 405.97 eV for DMRFB could be relevant to Cd–O binding, and 411.82 and 405.06 eV corresponded to the Cd–OH, demonstrating that precipitation was involved in metal ions binding (Chen et al. 2015). XRD analysis explored the possible precipitation mechanism, in which the typical $Cd(OH)_2$ peaks were indeed found in the XRD patterns of DMRFB (JCPDS PDF 80-1952) after adsorption (Additional file 1: Fig. S8E), further elucidating the Cd precipitation mechanism with the participation of mineral (Yin et al. 2020). The percentage of Cd atomic in DMRFB (2.37%) was more than that in FB (1.69%) (Additional file 1: Table S13), hinting toward the adsorption of numerous Cd ions onto DMRFB compared to FB. Above all, the addition of DOM-MR induced the strengthening of Cd adsorption by FB.

3.5 The composition characteristics of DOM and the mechanism of its binding with Cd(II)

3.5.1 The components of DOM identified by EEM-PARAFAC and their interactions with Cd(II)

Five individual components were identified from DOM through PARAFAC analysis, including three humic-like substances (C1, C2, and C3) and two protein-like substances (C4 and C5). The spectral characteristics and excitation and emission loadings of the components are illustrated in Additional file 1: Fig. S12. After comparing them with the Open Fluor online database, all components had a high degree of match with at least one other

study (Additional file 1: Table S14). The characteristics of DOM and its interactions with metals are crucial for the ecological risk assessment of metals in the environment (Zhang et al. 2022a, b, c). In the present study, the addition of Cd(II) caused significant quenching effects on DMR, as revealed by the fluorescence quenching curves (Fig. 7). These effects were mainly attributed to the pronounced fluorescence quenching of protein-like substances (C5), resulting in decreased fluorescence intensities. This suggested that the C5 component might form stable complexes with Cd(II). The quenching of protein-like components through complexation with metal ions has been observed in other studies (Huang et al. 2018; Wu et al. 2011). These findings strongly suggested that protein-like substances played a significant role in the complexation reaction between DOM derived from plant decomposition and Cd, which may explain the enhancement of the alleviation of Cd migration in aquatic systems (Yuan et al. 2015). The fluorescence intensity of the C1, C2, and C3 components did not show a significant change with the addition of additional Cd, indicating that the binding effect between Cd and fluorescent humic-like substances can be disregarded in the current study. All in all, the higher aromaticity and protein-like components in DOM played a vital role in the Cd binding process.

3.5.2 Insight into the molecular characteristics of DOM by FT-ICR MS

To delve deeper into the variations in molecular characteristics of DOM, detailed compositional differences among DMR, FB, and DMRFB were analyzed using FT-ICR MS. The van Krevelen (VK) diagram was employed to characterize the molecular composition of DOM in DMR, FB, and DMRFB samples, utilizing the classification criteria outlined in previous research studies (Huang et al. 2022; Liu et al. 2023) (Fig. 8A–C). FT-ICR MS analysis identified 7936, 1624, and 8704 DOM molecules across DMR, FB, and DMRFB samples, respectively (Additional file 1: Fig. S13C). Among them, lignins and protein/amino sugar were the most abundant molecules, accounting for 42.7–57.9% and 25.9–28.3% of all assigned molecules, respectively. Lipids and carbohydrates ranked second, representing 7.36–16.1% and 3.27–3.69%, respectively. Compared to FB, the number of identified compounds and peak intensities in DMRFB were significantly increased (Additional file 1: Fig. S13), indicating that the introduction of DMR enriched the molecular diversity of most DOM compounds in FB and enhanced the complexity of DOM. Figure 8G–I presents the relationship between the DBE value and the number of carbon atoms associated with the O/C ratio. Generally, a higher number of carbon atoms and a higher DBE value indicated larger molecular weight segments and more double bonds in the compounds (Wang et al. 2023). The higher DBE values were distributed in the lignins region, and they were more widely distributed in the DMRFB sample (Fig. 8D–F).

Considering the overall changes in molecular-level properties, we summarized the intensity-weighted average values (Additional file 1: Table S4). The AI_{mod} of DMRFB was significantly increased, indicating that unsaturated aromatic compounds were more stable and abundant, consistent with previous findings that DMRFB had higher aromaticity (Additional file 1: Fig. S8F). The higher DBE and NOSC in the DMRFB sample

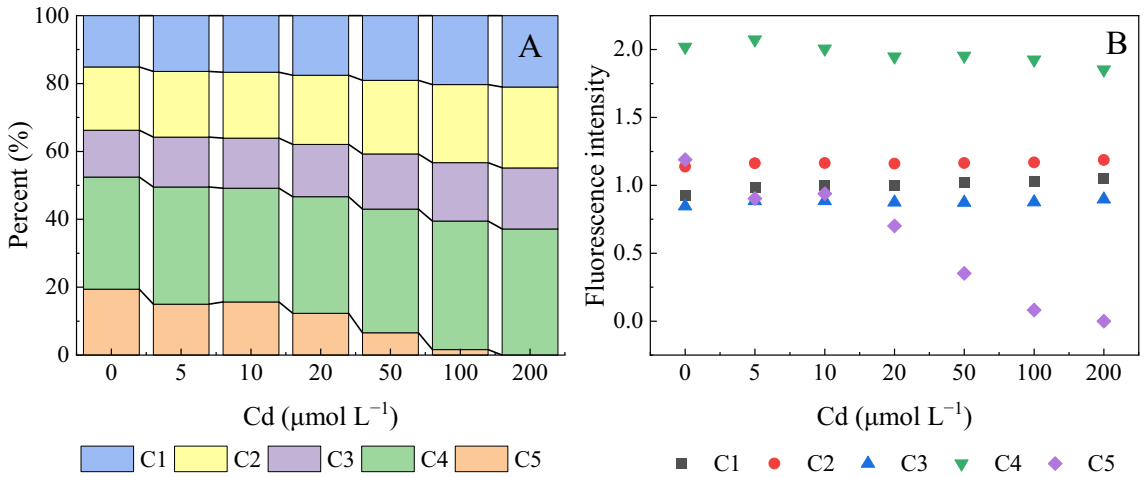

Fig. 7 The percent and fluorescence quenching curves of each PARAFAC-derived component titrated with Cd. **A** is percent of DOM components; **B** is fluorescence quenching curves of DOM components

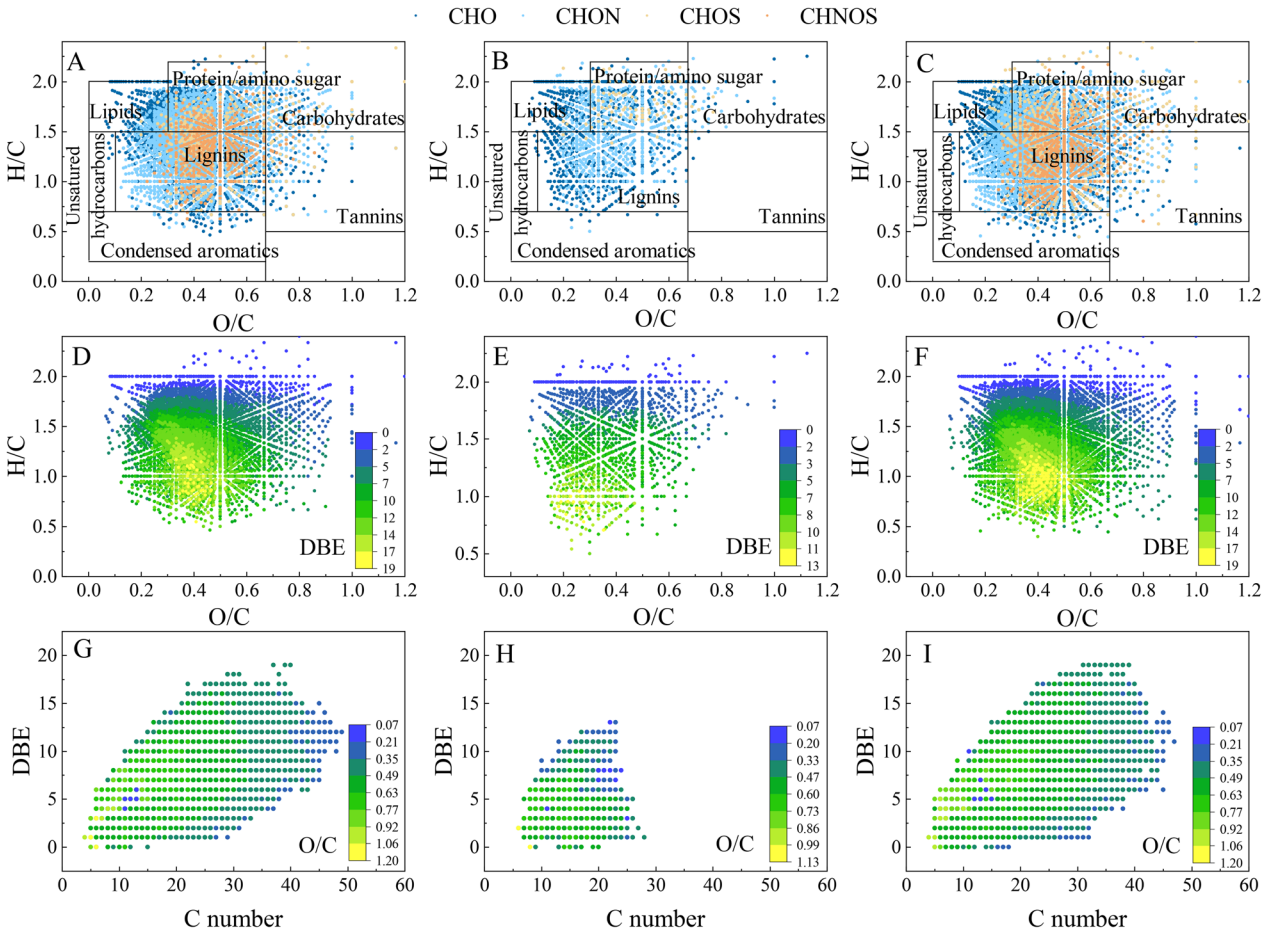

Fig. 8 Van Krevelen diagram of DMR, FB, and DMRFB (**A**, **B**, and **C**). **D**, **E**, and **F** are color-mapped based on the magnitude of DBE. **G**, **H**, and **I** are color-mapped based on the magnitude of the O/C ratio. **A**, **D**, **G**, DMR; **B**, **E**, **H**, FB; **C**, **F**, **I**, DMRFB

suggested a more complex composition of DOM, consisting of more unsaturated compounds (Huang et al. 2022). Similarly, the increased MW values also implied the transformation of small molecular DOM into larger molecules (Additional file 1: Table S4) (Zhang et al. 2019a, b, c). Additional file 1: Fig. S13C and D present the number and relative abundance of four main subgroups (CHO, CHNO, CHOS, CHNOS) in the DOMs of the three samples. The recalcitrant DOM formulas, particularly those belonging to the CHO and CHNO subgroups, were specifically plotted in the lignins/CRAM-like structural region highlighted in the VK diagram (Additional file 1: Fig. S14). Although lignins and CRAM compounds have similar O/C and H/C molar ratios, molecular weights, and DBE, they also exhibit different structural characteristics. In conclusion, the molecular diversity and complexity of DOM can be enhanced by the DMR, which may consequently impact the Cd binding process.

3.6 Overall findings and proposed mechanism

This study provided the basis for the observed extreme decrease in Cd concentration in rice plants under MRFB-S treatment, which can be largely attributed to the strengthening effect on stabilizing Cd by MR-S. MRFB-S transformed the Cd from active state to stable state and the increased Res-Cd might be $CdCO_3$ and $Cd(OH)_2$ supported by above results (Fig. 6, and Additional file 1: Fig. S8E). Large amounts of DOM released by MR had a positive influence on the Cd immobilization, as evidenced by the negative correlation between Avail-Cd and DOM in the correlation heat map and PLS-PM analysis (Additional file 1: Fig. S3 and Fig. 4B). A previous study has shown that DOM could interact with Cd through coordination, chelation, or complexation and decreased the Cd mobility, and further decreased Cd concentration in rice (Khan et al. 2017). In this process, the DOM with variable properties in complex soil environments played a significant role in controlling the migration and

transformation of Cd (Zhang et al. 2022a, b, c). The complex biological processes between DOM and microbial metabolism are considered to be the primary driving force behind DOM characteristics (Xu and Guo 2018). Therefore, higher microbial activity in paddy soils may influence the protein-like components in DOM, thereby affecting the interaction between Cd and DOM. Herein, the current study further provided the sufficient evidence that DOM was the key factor influencing the Cd availability (Fig. 4A). Wang et al (2022a, b, c) found that co-incorporation of Fe and DOM can form the Fe-OM complexes, which could stabilize bioavailable amorphous Fe and indirectly reduce Cd accumulation in brown rice. Similarly, co-using FB and MR in this study exhibited higher levels of Fe(II) in soil, resulting in promoting the Cd immobilization (Additional file 1: Fig. S4).

From another perspective, on the one hand, more available Fe (Fe(II)) in MRFB-S treatment could be absorbed by rice, thus suppressing the Cd uptake by brown rice through competition. The fact that more more Fe(II) of DMRFB was retained in the reaction system supported the above inference (Fig. 6E). On the other hand, more Fe(II) derived from the addition of MR contributed to the formation of more IP, and then prevented the Cd uptake by the rice plant. Meanwhile, a previous study showed that MV significantly increased the relative abundance of soil reducing-bacteria, further improving the formation of IP (Zheng et al. 2022), which is consistent with the present result about Fe plaque. Similarly, RS application could promote the greater microbial iron reduction (Yuan et al. 2019). In addition, FB could provide the Fe source for the IP formation and further controlled the Cd adsorption by rice (Sui et al. 2021). Consequently, co-incorporation of MR and FB exhibited the stronger capacity on decreasing Cd bioavailability. Furthermore, the dilution effect induced by the enhancement of rice biomass also helped to decrease the Cd contents in rice plants (Gasco et al. 2019; Han et al. 2006). Therefore, the above results indicated that the co-using MV, RS, and FB is excellent strategy that shows promise for remediation of Cd-contamination paddy soil.

The adsorption experiments manifested that DMRFB could improve the sorption performance of Cd(II) and the adsorption occurred mainly through chemisorption of monolayers. The chemical adsorption capacity of DMRFB was higher than that of FB primarily due to the increase in functional groups (including oxygen and aromatic functional groups) and the enhancement of negative charge both brought about by the presence of DOM. Four chemisorption mechanisms were proposed to explain why the DMRFB produced high Cd(II) adsorption capacity. (i) More oxygenated functional groups of DMRFB participated in the surface complexation, thus providing the possible of forming intricate compounds containing Cd (Qu et al. 2022b; Zheng et al. 2021). Interestingly, the levels of Ca-O-Cd complexes amened with DMRFB surpassed those treated with FB (Fig. 6D), indicating that the Cd and Ca groups exhibited a greater tendency to form complexes and become immobilized onto DMRFB compared to FB. Moreover, the aromatic components of DOM (protein-like) in DMRFB treatment readily formed with Cd to form stable complexes (Fig. 7). (ii) The mineral on the DMRFB and the rising pH of the reaction system affected the Cd(II) adsorption performance through the formation of precipitation (e.g., $Cd(OH)_2$ and $CdCO_3$) (Chen et al. 2020), which can be verified preliminarily by XRD and XPS analysis. (iii) More aromatic functional groups C=C and –CH can promote the coordination with Cd(II) through the cation (Cd)–π interactions. (iv) DMR introduced a large amount of Ca ions and K ions, and these abundant cations in DMRFB were conducive to ion exchange reactions with Cd(II) (Fig. 6D, Additional file 1: Figs. S7 and S8B, E).

Moreover, the physisorption induced by the DMRFB also played a key role in Cd immobilization. The rapid initial period demonstrated by the adsorption kinetic data proved the involvement of the physisorption mechanism in the Cd(II) adsorption (Ahmad et al. 2018). The physical adsorption capacity of DMRFB is superior to that of FB, primarily due to the higher specific surface area, aromaticity, and negative charge brought about by DOM. The physical adsorption process mainly included the following two specific mechanisms. (i) The more abundant mesoporous structures and higher S_{BET} in DMRFB provide access to the active adsorption sites for the adsorbates, facilitating the quick formation of an adsorption balance and improving the adsorption capacity (Li et al. 2017) (Table 1). (ii) The higher negative charge on the surface of DMRFB could easily capture the Cd ion via electrostatic attraction (Rajapaksha et al. 2016) (Table 1), which promoted the adsorption under DMRFB treatment. Additionally, DMRFB had high aromaticity, which is favorable for electrostatic sorption of Cd(II) (Thomas et al. 2020). Overall, the present study inferred that DOM-MR induced the higher negative charges, additional Cd active adsorption sites, and more surface functional groups, thereby facilitating the Cd(II) adsorption of DMRFB. This adsorption process involved the synergistic control of multiple mechanisms, including electrostatic attraction, pore adsorption, Cd(II)-π interactions, ion exchange, as well as the complexation of functional group and mineral precipitation.

FT-ICR MS and EEM-PARAFAC explained the possible mechanisms of Cd adsorption from the perspective of DOM molecular diversity. Lignins are complex biopolymers primarily consisting of alkoxy

or hydroxy-substituted aromatic structures linked by ether bonds (Yuan et al. 2017), while CRAM is mostly composed of carbonyl-containing species with isolated ketones and several carboxyl groups (Qi et al. 2022). The carboxyl-rich CRAM compounds can act as strong ligands for metal binding, promoting aggregation and gel formation through multiple coordination with metal cations, thereby affecting the bioavailability of metals (Hertkorn et al. 2006). In the current study, the DMRFB sample had the higher abundance of CRAM, being 1.13 and 8.22 times higher than DMR and FB, respectively (Additional file 1: Fig. S14). This might strengthen the reactions such as coordination and complexation between DOM and Cd ions. Proteins/amino sugars and lipids are compounds that contain negatively charged organic groups such as amino, thiol, hydroxyl, and carboxyl groups (Kranthi et al. 2018). These groups can effectively bind to Cd ions to form precipitates and enhance electrostatic adsorption interactions with Cd. EEM-PARAFAC revealed that proteins-like played a significant role in the complexation of Cd. Considering that proteins/amino sugars constituted a significant proportion of DOM components and the peak intensity of proteins in DMRFB samples was much higher compared to DMR and FB, it is inferred that protein components in DMRFB samples may be more extensively involved in the reaction with Cd. This finding is aligned with the fact that DMRFB was more favorable for the reaction with Cd and exhibited stronger Cd adsorption capacity. Additionally, the abundance of lipid, carbohydrate, and condensed aromatic compounds in DMRFB was significantly increased compared to FB. Carbohydrates are polyhydroxy aldehydes or ketones with multiple hydroxyl functional groups, which can interact with potential toxic elements and readily adsorb Cd(II) in solution (Kranthi et al. 2018). Condensed aromatics contain abundant carboxylic acid, carbonyl, hydroxyl, and ester groups, which play important roles in the adsorption of metal ions (Zhang et al. 2021).

In the current study, different sources and forms of organic inputs resulted in different distributions of DOM components in DMR, FB, and DMRFB. The finding is aligned with the hypothesis that common agricultural practices (e.g., straw incorporation and organic fertilizer application) may contribute to the presence of exogenous (terrestrial) characteristics in agricultural soil DOM (Zhang et al. 2022a, b, c). On the one hand, in the different components of DOM, the protein-like component played a crucial role in the adsorption process of Cd. On the other hand, a study has shown that DOM with more aromatic compounds and highly aromatized DOM had a stronger affinity for Cd (Cornu et al. 2011), which affected the binding between Cd and DOM. In this study, the overlap of DMR and FB increased the aromaticity of FB, which can be observed in FT-ICR MS and FT-IR (Fig. 8 and Additional file 1: Fig. S8F). The high degree of aromatization of DOM in DMRFB treatment might contribute to the adsorption of Cd(II), thus enhancing the Cd(II) adsorption performance (Chen et al. 2021a, b). Likewise, Xie et al. (2019) observed a negative linear relationship between water-soluble Cd and aromaticity. Therefore, the DOM from the decomposition of milk vetch and rice straw increased the richness and complexity of DOM molecules in the solution containing FB, especially lignins/CRAM and protein/amino sugar, which promoted the adsorption and fixation of Cd.

3.7 Environmental implications

In recent years, the trend of Cd pollution caused by soil degradation of agricultural land in southern China has increased. The important reason for the degradation of farmland was the emphasis on use rather than nourishment, and the means of farmland nourishment were seriously inadequate. Moreover, the management of Cd-contaminated soil was only focused on remediation, ignoring the endogenous regulation function of the soil. For example, although the meta-analyze has shown that the application of biochar can inhibit the uptake of Cd by various crops and has persistent remediation effects on soil Cd (Duan et al. 2023), long-term application of biochar may have adverse effects on the soil environment. This is primarily due to its non-specific adsorption characteristics, which can lead to issues like salinization. Ultimately, these adverse effects can hinder crop growth (Wang et al. 2020). Thus, it was essential to seek the path of simultaneous soil Cd pollution treatment and fertilization.

Substantial crop straws are harvested in China, yet the overall utilization efficiency is low and the phenomenon of resource wastage is severe (Jin et al. 2023; Ren et al. 2019). Thus, enhancing the integrated utilization of crop residues is significant. Previous researchers found that returning RS to the field not only reduced air pollution caused by straw burning, but also returned considerable amounts of nutrients to the soil and improved crop production (Yang et al. 2019; Zhou et al. 2023). Meanwhile, co-utilizing MV and RS is an innovative strategy in southern China to enhance their decomposition and consistent release of significant DOM into the soil for agricultural benefits (Zhou et al. 2020a). This study provided the vital evidence that the Cd(II) sorption was largely strengthened through adding the DOM derived from the co-decomposition of MV and RS, which might offer potential for the remediation of Cd-contaminated soil by combined green manure, rice straw, and passivated material in paddy fields. Furthermore, the superior Cd(II) adsorption performance of FB has achieved

high adsorption efficiency at lower dosages compared to previous studies, reducing the potential negative effects associated with large-dosage application of biochar (Sui et al. 2021; Sun et al. 2022). From another perspective, the improvement of different physicochemical properties of soil by co-using milk vetch, rice straw, and iron-modified also reflected its adaptability and superiority on soil fertilization.

4 Conclusion

This study showed that co-incorporating milk vetch, rice straw, and Fe-modified biochar improved soil nutrient, elevated the rice grain biomass, and decreased the Cd concentration in brown rice, achieving production without exceeding the safety limit. In addition, the DOM derived from the decomposition of MR exhibited certain diversity and complexity, with its main components (lignin/carboxylic-rich alicyclic molecules and protein/amino sugar) potentially involved in the adsorption of Cd. Correspondingly, Fe-modified biochar attained more negative charges, specific surface area, and functional groups due to the induction of the DOM, which strengthened the physisorption and chemisorption capacities of Cd(II) on Fe-modified biochar. Overall, co-using milk vetch, rice straw, and Fe-modified biochar is a promising practice to remediate Cd-polluted farmland. Nevertheless, dynamic soil conditions (e.g., pH, Eh, and microbial activities) at the field scale may induce interactions between FB and DOM derived from MR and the subsequent effects on the mobility of Cd, and thus deserve further study.

Supplementary Information

The online version contains supplementary material available at https://doi.org/10.1007/s42773-024-00313-6.

Additional file 1: Fig. S1. Adsorption capacity of different biochar. **Fig. S2.** Effect of Cd(II) equilibrium concentrations under different treatments. **Fig. S3.** Correlation heat map of Cd bioavailability and soil properties. (Blue and red represent negative and positive correlations, respectively. Darker colors represent higher correlations. *, $P<0.05$, **, $P<0.01$, ***, $P<0.001$). **Fig. S4.** Fe^{2+} concentrations in soil (LSD Test, $P < 0.05$). **Fig. S5.** Biomass of rice different tissues (LSD Test, $P < 0.05$). **Fig. S6.** SEM-EDS mapping images of FB and DMRFB before Cd(II) adsorption (A, FB; B, DMRFB). **Fig. S7.** FT-IR spectrum (A: DMR, FB, and DMRFB) and XRD profile of DMR (B: DMR). **Fig. S8.** EDS-mapping images (A: FB-Cd and B: DMRFB-Cd), N_2 adsorption-desorption isothermal curve and pore-size distributions (C and D), and XRD and FT-IR profiles of FB and DMRFB (E and F). **Fig. S9.** Effect of Cd(II) adsorption at different decomposition time. **Fig. S10.** The linear correlation between pH and Cd(II) equilibrium concentrations. **Fig. S11.** Desorption efficiency at different initial Cd(II) concentrations. **Fig. S12.** Five fluorescent components in DOM identified by EEM-PARAFAC analysis. A, Spectral characteristics of five identified components (The contour lines and colors represent the relative intensity of emission (yellow and navy blue correspond to most and least intense, respectively). B, Excitation and emission loadings of five components from DOM. **Fig. S13.** Numbers and intensities of the identified DOM formulae by elemental groups (A, number; B, intensity) and biochemical classes (C, number; D, intensity) in the samples of DMR, FB, and DMRFB. **Fig. S14.** Van Krevelen diagram of the carboxylic-rich alicyclic molecules (CRAM) (A, DMR; B, FB; C, DMRFB). **Table S1.** The experimental design for pot trial. Note: Chinese milk vetch and rice straw were calculated and applied to the soil using fresh and dry weights, respectively. **Table S2.** The basic physicochemical properties of studied soil. **Table S3.** Compound class and boundaries of regions in van Krevelen diagrams. **Table S4.** Molecular properties of DOM in different samples. **Table S5.** The resulting information of Shapiro-Wilk analysis. **Table S6.** Effects of different treatments on soil chemical properties in pot experiments. **Table S7.** The adsorption isothermal model parameters on FB and DMRFB for Cd(II). **Table S8.** Summary of for modified biochar adsorption capacity on Cd(II). **Table S9.** The kinetic model parameters of adsorption. **Table S10.** Thermodynamic parameters for Cd(II) adsorption by FB and DMRFB. **Table S11.** The activation energy of FB and DMRFB. **Table 12.** The concentrations of acidic functional groups. **Table S13.** The percentages of atomic in XPS. **Table S14.** Identities and related references for similar components using the OpenFluor database.

Acknowledgements

We thank Dr. Xing Xia (Anhui Agricultural University) who provided technical assistance and constructive feedback on this manuscript. Thanks to the XPS support from Shiyanjia Lab (www.shiyanjia.com).

Author contributions

TL: Data curation, Formal analysis, Methodology, Visualization, and Roles/Writing—original draft; GZ: Methodology, Investigation and Validation, Writing—review and editing; DC: Methodology, Writing—review and editing; ZM: Data curation and Formal analysis; SG: Investigation and Validation; JN: Investigation and Resources; YL: Investigation and Project administration; YL: Investigation and Project administration; HF: Funding acquisition, Investigation and Project administration; Chunqin Zou: Conceptualization and Supervision, Supervision, and Writing—review and editing; Weidong Cao: Conceptualization and Supervision, Funding acquisition, Project administration, Resources, Supervision, and Writing—review and editing.

Funding

This research was funded by the National Key Research and Development Program of China (2021YFD1700200), the earmarked fund for CARS-Green manure (CARS-22), and the Agricultural Science and Technology Innovation Program of Chinese Academy of Agricultural Sciences (ASTIP).

Availability of data and materials

The datasets used or analyzed during the current study are available from the corresponding author on reasonable request.

Declarations

Competing interests

The authors have no competing interests to declare that are relevant to the content of this article.

Author details

[1]State Key Laboratory of Efficient Utilization of Arid and Semi-Arid Arable Land in Northern China, Institute of Agricultural Resources and Regional Planning, Chinese Academy of Agricultural Sciences, Beijing 100081, China. [2]Key Laboratory of Plant-Soil Interactions, Ministry of Education, College of Resources and Environmental Sciences, National Academy of Agriculture Green Development, China Agricultural University, Beijing 100193, China. [3]Anhui Province Key Lab of Farmland Ecological Conservation and Nutrient Utilization, Anhui Province Engineering and Technology Research Center of Intelligent Manufacture and Efficient Utilization of Green Phosphorus Fertilizer, College of Resources and Environment, Anhui Agricultural University, Hefei 230036, China. [4]College of Resources and Environmental Sciences, Nanjing Agricultural University, Nanjing 210095, China. [5]Soil and Fertilizer Institute of Hunan Province, Hunan Academy of Agricultural Sciences, Changsha 410125, China.

Received: 25 August 2023 Revised: 7 February 2024 Accepted: 23 February 2024
Published online: 25 March 2024

References

Abbas T, Rizwan M, Ali S, Zia-Ur-Rehman M, Farooq Qayyum M, Abbas F, Hannan F, Rinklebe J, Sik Ok Y (2017) Effect of biochar on cadmium bioavailability and uptake in wheat (Triticum aestivum L.) grown in a soil with aged contamination. Ecotoxicol Environ Saf 140:37–47. https://doi.org/10.1016/j.ecoenv.2017.02.028

Ahmad Z, Gao B, Mosa A, Yu H, Yin X, Bashir A, Ghoveisi H, Wang S (2018) Removal of Cu(II), Cd(II) and Pb(II) ions from aqueous solutions by biochars derived from potassium-rich biomass. J Clean Prod 180:437–449. https://doi.org/10.1016/j.jclepro.2018.01.133

Antoniadis V, Levizou E, Shaheen SM, Ok YS, Sebastian A, Baum C, Prasad MNV, Wenzel WW, Rinklebe J (2017) Trace elements in the soil-plant interface: phytoavailability, translocation, and phytoremediation—a review. Earth Sci Rev 171:621–645. https://doi.org/10.1016/j.earscirev.2017.06.005

Arabi Z, Rinklebe J, El-Naggar A, Hou D, Sarmah AK, Moreno-Jimenez E (2021) (Im)mobilization of arsenic, chromium, and nickel in soils via biochar: a meta-analysis. Environ Pollut 286:117199. https://doi.org/10.1016/j.envpol.2021.117199

Bao SD (2000) Soil agricultural chemical analysis method. China Agricultural Science and Technology Press 1–495.

Boehm HP (1994) Some aspects of the surface chemistry of carbon blacks and other carbons. Carbon 32(5):759–769. https://doi.org/10.1016/0008-6223(94)90031-0

Bolan N, Kunhikrishnan A, Thangarajan R, Kumpiene J, Park J, Makino T, Kirkham MB, Scheckel K (2014) Remediation of heavy metal(loid) s contaminated soils—to mobilize or to immobilize? J Hazard Mater 266:141–166. https://doi.org/10.1016/j.jhazmat.2013.12.018

Borggaard OK, Holm PE, Strobel BW (2019) Potential of dissolved organic matter (DOM) to extract As, Cd Co, Cr, Cu, Ni, Pb and Zn from polluted soils: a review. Geoderma 343:235–246. https://doi.org/10.1016/j.geoderma.2019.02.041

Chen T, Zhou Z, Han R, Meng R, Wang H, Lu W (2015) Adsorption of cadmium by biochar derived from municipal sewage sludge: impact factors and adsorption mechanism. Chemosphere 134:286–293. https://doi.org/10.1016/j.chemosphere.2015.04.052

Chen D, Wang X, Wang X, Feng K, Su J, Dong J (2020) The mechanism of cadmium sorption by sulphur-modified wheat straw biochar and its application cadmium-contaminated soil. Sci Total Environ 714:136550. https://doi.org/10.1016/j.scitotenv.2020.136550

Chen M, Ding S, Li C, Tang Y, Fan X, Xu H, Tsang DCW, Zhang C (2021a) High cadmium pollution from sediments in a eutrophic lake caused by dissolved organic matter complexation and reduction of manganese oxide. Water Res 190:116711. https://doi.org/10.1016/j.watres.2020.116711

Chen Z, Pei J, Wei Z, Ruan X, Hua Y, Xu W, Zhang C, Liu T, Guo Y (2021b) A novel maize biochar-based compound fertilizer for immobilizing cadmium and improving soil quality and maize growth. Environ Pollut 277:116455. https://doi.org/10.1016/j.envpol.2021.116455

Cornu JY, Schneider A, Jezequel K, Denaix L (2011) Modelling the complexation of Cd in soil solution at different temperatures using the UV-absorbance of dissolved organic matter. Geoderma 162(1–2):65–70. https://doi.org/10.1016/j.geoderma.2011.01.005

Duan Z, Chen C, Ni C, Xiong J, Wang Z, Cai J, Tan W (2023) How different is the remediation effect of biochar for cadmium contaminated soil in various cropping systems? A global meta-analysis. J Hazard Mater 448:130939. https://doi.org/10.1016/j.jhazmat.2023.130939

El-Naggar A, Chen Z, Jiang W, Cai Y, Chang SX (2022) Biochar effectively remediates Cd contamination in acidic or coarse- and medium-textured soils: a global meta-analysis. Chem Eng J 442:136225. https://doi.org/10.1016/j.cej.2022.136225

Feng Z, Fan Z, Song H, Li K, Lu H, Liu Y, Cheng F (2021) Biochar induced changes of soil dissolved organic matter: the release and adsorption of dissolved organic matter by biochar and soil. Sci Total Environ 783:147091. https://doi.org/10.1016/j.scitotenv.2021.147091

Gao SJ, Zhou GP, Chang D, Liang H, Nie J, Liao YL, Lu YH, Xu CX, Liu J, Wu J, Han S, Wang H, Liu CZ, Lv YH, Huang YB, He CM, Geng MJ, Wang JH, He TG, Li ZY, Liang H, Li S, Rees RM, Thorup-Kristensen K, Cao WD (2023) Southern China can produce more high-quality rice with less N by green manuring. Resour Conserv Recycl 196:107025. https://doi.org/10.1016/j.resconrec.2023.107025

Gasco G, Alvarez ML, Paz-Ferreiro J, Mendez A (2019) Combining phytoextraction by Brassica napus and biochar amendment for the remediation of a mining soil in Riotinto (Spain). Chemosphere 231:562–570. https://doi.org/10.1016/j.chemosphere.2019.05.168

Han SH, Lee JC, Oh CY, Kim PG (2006) Alleviation of Cd toxicity by composted sewage sludge in Cd-treated Schmidt birch (Betula schmidtii) seedlings. Chemosphere 65(4):541–546. https://doi.org/10.1016/j.chemosphere.2006.02.049

He R, Peng Z, Lyu H, Huang H, Nan Q, Tang J (2018) Synthesis and characterization of an iron-impregnated biochar for aqueous arsenic removal. Sci Total Environ 612:1177–1186. https://doi.org/10.1016/j.scitotenv.2017.09.016

Hertkorn N, Benner R, Frommberger M, Schmitt-Kopplin P, Witt M, Kaiser K, Kettrup A, Hedges JI (2006) Characterization of a major refractory component of marine dissolved organic matter. Geochim Cosmochim Acta 70(12):2990–3010. https://doi.org/10.1016/j.gca.2006.03.021

Huang M, Li Z, Huang B, Luo N, Zhang Q, Zhai X, Zeng G (2018) Investigating binding characteristics of cadmium and copper to DOM derived from compost and rice straw using EEM-PARAFAC combined with two-dimensional FTIR correlation analyses. J Hazard Mater 344:539–548. https://doi.org/10.1016/j.jhazmat.2017.10.022

Huang M, Zhou M, Li Z, Ding X, Wen J, Jin C, Wang L, Xiao L, Chen J (2022) How do drying-wetting cycles influence availability of heavy metals in sediment? A perspective from DOM molecular composition. Water Res 220:118671. https://doi.org/10.1016/j.watres.2022.118671

Hunt JF, Ohno T (2007) Characterization of fresh and decomposed dissolved organic matter using excitation-emission matrix fluorescence spectroscopy and multiway analysis. J Agric Food Chem 55:2121–2128. https://doi.org/10.1021/jf063336m

Irshad MK, Noman A, Wang Y, Yin Y, Chen C, Shang J (2022) Goethite modified biochar simultaneously mitigates the arsenic and cadmium accumulation in paddy rice (Oryza sativa) L. Environ Res 206:112238. https://doi.org/10.1016/j.envres.2021.112238

Jin K, Zhang S, Yang Y, Chen X, Wang S, Li T, Wang Y (2023) Evaluation of water-carbon-ecological footprints and its spatial–temporal pattern in the central plains urban agglomeration. Ecol Ind 155:110982. https://doi.org/10.1016/j.ecolind.2023.110982

Khan MA, Khan S, Khan A, Alam M (2017) Soil contamination with cadmium, consequences and remediation using organic amendments. Sci Total Environ 601–602:1591–1605. https://doi.org/10.1016/j.scitotenv.2017.06.030

Kranthi KR, Sardar UR, Bhargavi E, Devi I, Bhunia B, Tiwari ON (2018) Advances in exopolysaccharides based bioremediation of heavy metals in soil and water: a critical review. Carbohydr Polym 199:353–364. https://doi.org/10.1016/j.carbpol.2018.07.037

Li B, Yang L, Wang CQ, Zhang QP, Liu QC, Li YD, Xiao R (2017) Adsorption of Cd(II) from aqueous solutions by rape straw biochar derived from different modification processes. Chemosphere 175:332–340. https://doi.org/10.1016/j.chemosphere.2017.02.061

Liang T, Li L, Zhu C, Liu X, Li H, Su Q, Ye J, Geng B, Tian Y, Sardar MF, Huang X, Li F (2020) Adsorption of As(V) by the novel and efficient adsorbent cerium-manganese modified biochar. Water 12(10):2720. https://doi.org/10.3390/w12102720

Liang T, Zhou G, Chang D, Wang Y, Gao S, Nie J, Liao Y, Lu Y, Zou C, Cao W (2022) Co-incorporation of Chinese milk vetch (Astragalus sinicus L.), rice straw, and biochar strengthens the mitigation of Cd uptake by rice (Oryza sativa L.). Sci Total Environ 850:158060. https://doi.org/10.1016/j.scitotenv.2022.158060

Liu G, Meng J, Huang Y, Dai Z, Tang C, Xu J (2020) Effects of carbide slag, lodestone and biochar on the immobilization, plant uptake and translocation of As and Cd in a contaminated paddy soil. Environ Pollut 266(Pt 1):115194. https://doi.org/10.1016/j.envpol.2020.115194

Liu L, Du L, Lu S, Yang B, Zhao X, Wu D, Fei X, He H, Wang D (2023) Molecular insight into DOM fate using EEM-PARAFAC and FT-ICR MS and concomitant heavy metal behaviors in biologically treated landfill leachate during coagulation: Al speciation dependence. J Hazard Mater 460:132374. https://doi.org/10.1016/j.jhazmat.2023.132374

Lu RK (2000) Analysis methods of soil agricultural chemistry. China Agricultural Science and Technology Publishing House in Chinese

Lyu P, Li L, Huang X, Wang G, Zhu C (2022a) Pre-magnetic bamboo biochar cross-linked CaMgAl layered double-hydroxide composite: high-efficiency removal of As(III) and Cd(II) from aqueous solutions and insight into the mechanism of simultaneous purification. Sci Total Environ 823:153743. https://doi.org/10.1016/j.scitotenv.2022.153743

Lyu P, Li L, Huang X, Xie J, Ye J, Tian Y, Huang J, Zhu C (2022b) Ternary Ca-Mg-Al layered double-hydroxides for synergistic remediation of As, Cd, and Pb from both contaminated soil and groundwater: characteristics, effectiveness, and immobilization mechanisms. J Hazard Mater 442:130030. https://doi.org/10.1016/j.jhazmat.2022.130030

Matong JM, Nyaba L, Nomngongo PN (2016) Fractionation of trace elements in agricultural soils using ultrasound assisted sequential extraction prior to inductively coupled plasma mass spectrometric determination. Chemosphere 154:249–257. https://doi.org/10.1016/j.chemosphere.2016.03.123

Min T, Luo T, Chen L, Lu W, Wang Y, Cheng L, Ru S, Li J (2021) Effect of dissolved organic matter on the phytoremediation of Cd-contaminated soil by cotton. Ecotoxicol Environ Saf 226:112842. https://doi.org/10.1016/j.ecoenv.2021.112842

Mujtaba Munir MA, Liu G, Yousaf B, Ali MU, Cheema AI, Rashid MS, Rehman A (2020) Bamboo-biochar and hydrothermally treated-coal mediated geochemical speciation, transformation and uptake of Cd, Cr, and Pb in a polymetal(iod)s-contaminated mine soil. Environ Pollut 265(Pt A):114816. https://doi.org/10.1016/j.envpol.2020.114816

Ok YS, Rinklebe J, Hou D, Tsang DCW, Tack FMG (2020) Soil and groundwater remediation technologies: a practical guide. CRC Press. https://doi.org/10.1201/9780429322563

Palansooriya KN, Shaheen SM, Chen SS, Tsang DCW, Hashimoto Y, Hou D, Bolan NS, Rinklebe J, Ok YS (2020) Soil amendments for immobilization of potentially toxic elements in contaminated soils: a critical review. Environ Int 134:105046. https://doi.org/10.1016/j.envint.2019.105046

Plaza C, Brunetti G, Senesi N, Polo A (2006) Molecular and quantitative analysis of metal ion binding to humic acids from sewage sludge and sludge-amended soils by fluorescence spectroscopy. Environ Sci Technol 40(3):917–923. https://doi.org/10.1021/es051687w

Qi Y, Ma C, Chen S, Ge J, Hu Q, Li SL, Volmer DA, Fu P (2021) Online liquid chromatography and FT-ICR MS enable advanced separation and profiling of organosulfates in dissolved organic matter. ACS ES&T Water 1(8):1975–1982. https://doi.org/10.1021/acsestwater.1c00162

Qi Y, Xie Q, Wang J-J, He D, Bao H, Fu QL, Su S, Sheng M, Li SL, Volmer DA, Wu F, Jiang G, Liu CQ, Fu P (2022) Deciphering dissolved organic matter by Fourier transform ion cyclotron resonance mass spectrometry (FT-ICR MS): from bulk to fractions and individuals. Carbon Res. https://doi.org/10.1007/s44246-022-00002-8

Qiao JT, Liu TX, Wang XQ, Li FB, Lv YH, Cui JH, Zeng XD, Yuan YZ, Liu CP (2018) Simultaneous alleviation of cadmium and arsenic accumulation in rice by applying zero-valent iron and biochar to contaminated paddy soils. Chemosphere 195:260–271. https://doi.org/10.1016/j.chemosphere.2017.12.081

Qu J, Dong M, Bi F, Tao Y, Wang L, Jiang Z, Zhang G, Zhang B, Zhang Y (2022a) Microwave-assisted one-pot synthesis of β-cyclodextrin modified biochar for stabilization of Cd and Pb in soil. J Clean Prod 346:131165. https://doi.org/10.1016/j.jclepro.2022.131165

Qu J, Yuan Y, Zhang X, Wang L, Tao Y, Jiang Z, Yu H, Dong M, Zhang Y (2022b) Stabilization of lead and cadmium in soil by sulfur-iron functionalized biochar: performance, mechanisms and microbial community evolution. J Hazard Mater 425:127876. https://doi.org/10.1016/j.jhazmat.2021.127876

Rajapaksha AU, Chen SS, Tsang DC, Zhang M, Vithanage M, Mandal S, Gao B, Bolan NS, Ok YS (2016) Engineered/designer biochar for contaminant removal/immobilization from soil and water: potential and implication of biochar modification. Chemosphere 148:276–291. https://doi.org/10.1016/j.chemosphere.2016.01.043

Ren J, Yu P, Xu X (2019) Straw utilization in China—status and recommendations. Sustainability 11(6):1762. https://doi.org/10.3390/su11061762

Shaheen SM, Natasha MA, El-Naggar A, Faysal Hossain M, Abdelrahman H, Khan Niazi N, Shahid M, Zhang T, Fai Tsang Y, Trakal L, Wang S, Rinklebe J (2022) Manganese oxide-modified biochar: production, characterization and applications for the removal of pollutants from aqueous environments—a review. Bioresour Technol 346:126581. https://doi.org/10.1016/j.biortech.2021.126581

Shi Y, Zhao Z, Zhong Y, Hou H, Chen J, Wang L, Wu X, Crittenden JC (2022) Synergistic effect of floatable hydroxyapatite-modified biochar adsorption and low-level CaCl2 leaching on Cd removal from paddy soil. Sci Total Environ 807(Pt 2):150872. https://doi.org/10.1016/j.scitotenv.2021.150872

Stedmon CA, Bro R (2008) Characterizing dissolved organic matter fluorescence with parallel factor analysis: a tutorial. Limnol Oceanogr Methods 6(11):572–579. https://doi.org/10.4319/lom.2008.6.572

Sui F, Kang Y, Wu H, Li H, Wang J, Joseph S, Munroe P, Li L, Pan G (2021) Effects of iron-modified biochar with S-rich and Si-rich feedstocks on Cd immobilization in the soil-rice system. Ecotoxicol Environ Saf 225:112764. https://doi.org/10.1016/j.ecoenv.2021.112764

Sun T, Xu Y, Sun Y, Wang L, Liang X, Zheng S (2021) Cd immobilization and soil quality under Fe-modified biochar in weakly alkaline soil. Chemosphere 280:130606. https://doi.org/10.1016/j.chemosphere.2021.130606

Sun L, Gong P, Sun Y, Qin Q, Song K, Ye J, Zhang H, Zhou B, Xue Y (2022) Modified chicken manure biochar enhanced the adsorption for Cd(2+) in aqueous and immobilization of Cd in contaminated agricultural soil. Sci Total Environ 851(Pt 2):158252. https://doi.org/10.1016/j.scitotenv.2022.158252

Sun T, Sun Y, Xu Y, Wang L, Liang X (2023) Effective removal of Hg2+ and Cd2+ in aqueous systems by Fe–Mn oxide modified biochar: a combined experimental and DFT calculation. Desalination 549:116306. https://doi.org/10.1016/j.desal.2022.116306

Sutherland RA, Tack FMG (2002) Determination of Al, Cu, Fe, Mn, Pb and Zn in certified reference materials using the optimized BCR sequential extraction procedure. Anal Chim Acta 454(2):249–257. https://doi.org/10.1016/S0003-2670(01)01553-7

Tan Y, Wan X, Ni X, Wang L, Zhou T, Sun H, Wang N, Yin X (2022) Efficient removal of Cd (II) from aqueous solution by chitosan modified kiwi branch biochar. Chemosphere 289:133251. https://doi.org/10.1016/j.chemosphere.2021.133251

Thomas E, Borchard N, Sarmiento C, Atkinson R, Ladd B (2020) Key factors determining biochar sorption capacity for metal contaminants: a literature synthesis. Biochar 2(2):151–163. https://doi.org/10.1007/s42773-020-00053-3

Trakal L, Veselska V, Safarik I, Vitkova M, Cihalova S, Komarek M (2016) Lead and cadmium sorption mechanisms on magnetically modified biochars. Bioresour Technol 203:318–324. https://doi.org/10.1016/j.biortech.2015.12.056

Wan X, Li C, Parikh SJ (2020) Simultaneous removal of arsenic, cadmium, and lead from soil by iron-modified magnetic biochar. Environ Pollut 261:114157. https://doi.org/10.1016/j.envpol.2020.114157

Wang P, Chen H, Kopittke PM, Zhao FJ (2019) Cadmium contamination in agricultural soils of China and the impact on food safety. Environ Pollut 249:1038–1048. https://doi.org/10.1016/j.envpol.2019.03.063

Wang Y, Liu Y, Zhan W, Zheng K, Wang J, Zhang C, Chen R (2020) Stabilization of heavy metal-contaminated soils by biochar: challenges and recommendations. Sci Total Environ 729:139060. https://doi.org/10.1016/j.scitotenv.2020.139060

Wang J, Wang Y, Wang J, Du G, Khan KY, Song Y, Cui X, Cheng Z, Yan B, Chen G (2022a) Comparison of cadmium adsorption by hydrochar and pyrochar derived from Napier grass. Chemosphere 308(Pt 3):136389. https://doi.org/10.1016/j.chemosphere.2022.136389

Wang X, Du Y, Li F, Fang L, Pang T, Wu W, Liu C, Chen L (2022b) Unique feature of Fe-OM complexes for limiting Cd accumulation in grains by target-regulating gene expression in rice tissues. J Hazard Mater 424(Pt A):127361. https://doi.org/10.1016/j.jhazmat.2021.127361

Wang Y, Liang H, Li S, Zhang Z, Liao Y, Lu Y, Zhou G, Gao S, Nie J, Cao W (2022c) Co-utilizing milk vetch, rice straw, and lime reduces the Cd accumulation of rice grain in two paddy soils in south China. Sci Total Environ 806(Pt 2):150622. https://doi.org/10.1016/j.scitotenv.2021.150622

Wang Y, Li N, Fu Q, Cheng Z, Song Y, Yan B, Chen G, Hou LA, Wang S (2023) Conversion and impact of dissolved organic matters in a heterogeneous catalytic peroxymonosulfate system for pollutant degradation. Water Res 241:120166. https://doi.org/10.1016/j.watres.2023.120166

Wu J, Zhang H, He P-J, Shao L-M (2011) Insight into the heavy metal binding potential of dissolved organic matter in MSW leachate using EEM quenching combined with PARAFAC analysis. Water Res 45(4):1711–1719. https://doi.org/10.1016/j.watres.2010.11.022

Wu J, Li Z, Huang D, Liu X, Tang C, Parikh SJ, Xu J (2020) A novel calcium-based magnetic biochar is effective in stabilization of arsenic and cadmium co-contamination in aerobic soils. J Hazard Mater 387:122010. https://doi.org/10.1016/j.jhazmat.2019.122010

Xia X, Wang J, Hu Y, Liu J, Darma AI, Jin L, Han H, He C, Yang J (2022) Molecular insights into roles of dissolved organic matter in Cr(III) immobilization by coprecipitation with Fe(III) Probed by STXM-ptychography and XANES spectroscopy. Environ Sci Technol 56(4):2432–2442. https://doi.org/10.1021/acs.est.1c07528

Xie J, Dong A, Liu J, Su J, Hu P, Xu C, Chen J, Wu Q (2019) Relevance of dissolved organic matter generated from green manuring of Chinese milk vetch in relation to water-soluble cadmium. Environ Sci Pollut Res Int 26(16):16409–16421. https://doi.org/10.1007/s11356-019-05114-0

Xu H, Guo L (2018) Intriguing changes in molecular size and composition of dissolved organic matter induced by microbial degradation and self-assembly. Water Res 135:187–194. https://doi.org/10.1016/j.watres.2018.02.016

Yang L, Zhou X, Liao Y, Lu Y, Nie J, Cao W (2019) Co-incorporation of rice straw and green manure benefits rice yield and nutrient uptake. Crop Sci 59(2):749–759. https://doi.org/10.2135/cropsci2018.07.0427

Yang W, Zhou H, Gu J, Liao B, Zhang J, Wu P (2020) Application of rapeseed residue increases soil organic matter, microbial biomass, and enzyme activity and mitigates cadmium pollution risk in paddy fields. Environ Pollut 264:114681. https://doi.org/10.1016/j.envpol.2020.114681

Yin D, Wang X, Chen C, Peng B, Tan C, Li H (2016) Varying effect of biochar on Cd, Pb and As mobility in a multi-metal contaminated paddy soil. Chemosphere 152:196–206. https://doi.org/10.1016/j.chemosphere.2016.01.044

Yin D, Wang X, Peng B, Tan C, Ma LQ (2017) Effect of biochar and Fe-biochar on Cd and As mobility and transfer in soil-rice system. Chemosphere 186:928–937. https://doi.org/10.1016/j.chemosphere.2017.07.126

Yin G, Song X, Tao L, Sarkar B, Sarmah AK, Zhang W, Lin Q, Xiao R, Liu Q, Wang H (2020) Novel Fe-Mn binary oxide-biochar as an adsorbent for removing Cd(II) from aqueous solutions. Chem Eng J 389:124465. https://doi.org/10.1016/j.cej.2020.124465

Yuan DH, Guo XJ, Wen L, He LS, Wang JG, Li JQ (2015) Detection of Copper (II) and Cadmium (II) binding to dissolved organic matter from macrophyte decomposition by fluorescence excitation-emission matrix spectra combined with parallel factor analysis. Environ Pollut 204:152–160. https://doi.org/10.1016/j.envpol.2015.04.030

Yuan Z, He C, Shi Q, Xu C, Li Z, Wang C, Zhao H, Ni J (2017) Molecular insights into the transformation of dissolved organic matter in landfill leachate concentrate during biodegradation and coagulation processes using ESI FT-ICR MS. Environ Sci Technol 51(14):8110–8118. https://doi.org/10.1021/acs.est.7b02194

Yuan C, Li F, Cao W, Yang Z, Hu M, Sun W (2019) Cadmium solubility in paddy soil amended with organic matter, sulfate, and iron oxide in alternative watering conditions. J Hazard Mater 378:120672. https://doi.org/10.1016/j.jhazmat.2019.05.065

Zhang Q, Zhang L, Liu T, Liu B, Huang D, Zhu Q, Xu C (2018) The influence of liming on cadmium accumulation in rice grains via iron-reducing bacteria. Sci Total Environ 645:109–118. https://doi.org/10.1016/j.scitotenv.2018.06.316

Zhang B, Shan C, Hao Z, Liu J, Wu B, Pan B (2019a) Transformation of dissolved organic matter during full-scale treatment of integrated chemical wastewater: molecular composition correlated with spectral indexes and acute toxicity. Water Res 157:472–482. https://doi.org/10.1016/j.watres.2019.04.002

Zhang Q, Chen H, Xu C, Zhu H, Zhu Q (2019b) Heavy metal uptake in rice is regulated by pH-dependent iron plaque formation and the expression of the metal transporter genes. Environ Exp Bot 162:392–398. https://doi.org/10.1016/j.envexpbot.2019.03.004

Zhang R, Huang Q, Yan T, Yang J, Zheng Y, Li H, Li M (2019c) Effects of intercropping mulch on the content and composition of soil dissolved organic matter in apple orchard on the loess plateau. J Environ Manage 250:109531

Zhang JY, Zhou H, Gu JF, Huang F, Yang WJ, Wang SL, Yuan TY, Liao BH (2020a) Effects of nano-Fe3O4-modified biochar on iron plaque formation and Cd accumulation in rice (Oryza sativa L.). Environ Pollut 260:113970. https://doi.org/10.1016/j.envpol.2020.113970

Zhang S, Deng Y, Fu S, Xu M, Zhu P, Liang Y, Yin H, Jiang L, Bai L, Liu X, Jiang H, Liu H (2020b) Reduction mechanism of Cd accumulation in rice grain by Chinese milk vetch residue: Insight into microbial community. Ecotoxicol Environ Saf 202:110908. https://doi.org/10.1016/j.ecoenv.2020.110908

Zhang H, Heal K, Zhu X, Tigabu M, Xue Y, Zhou C (2021) Tolerance and detoxification mechanisms to cadmium stress by hyperaccumulator Erigeron annuus include molecule synthesis in root exudate. Ecotoxicol Environ Saf 219:112359. https://doi.org/10.1016/j.ecoenv.2021.112359

Zhang P, Xue B, Jiao L, Meng X, Zhang L, Li B, Sun H (2022a) Preparation of ball-milled phosphorus-loaded biochar and its highly effective remediation for Cd- and Pb-contaminated alkaline soil. Sci Total Environ 813:152648. https://doi.org/10.1016/j.scitotenv.2021.152648

Zhang X, Li Y, Ye J, Chen Z, Ren D, Zhang S (2022b) The spectral characteristics and cadmium complexation of soil dissolved organic matter in a wide range of forest lands. Environ Pollut 299:118834. https://doi.org/10.1016/j.envpol.2022.118834

Zhang Z, Li Y, Zong Y, Yu J, Ding H, Kong Y, Ma J, Ding L (2022c) Efficient removal of cadmium by salts modified-biochar: performance assessment, theoretical calculation, and quantitative mechanism analysis. Bioresour Technol 361:127717. https://doi.org/10.1016/j.biortech.2022.127717

Zhao M, Liu X, Li Z, Liang X, Wang Z, Zhang C, Liu W, Liu R, Zhao Y (2020) Inhibition effect of sulfur on Cd activity in soil-rice system and its mechanism. J Hazard Mater 407:124647. https://doi.org/10.1016/j.jhazmat.2020.124647

Zheng X, Ma X, Hua Y, Li D, Xiang J, Song W, Dong J (2021) Nitric acid-modified hydrochar enhance Cd(2+) sorption capacity and reduce the Cd(2+) accumulation in rice. Chemosphere 284:131261. https://doi.org/10.1016/j.chemosphere.2021.131261

Zheng S, Liao Y, Xu C, Wang Y, Zhang Q, Zhu Q, Zhu H, Sun Y, Zhou Y, Zhong D, Huang D (2022) Milk vetch returning reduces rice grain Cd concentration in paddy fields: roles of iron plaque and soil reducing-bacteria. Chemosphere 308(Pt 1):136158. https://doi.org/10.1016/j.chemosphere.2022.136158

Zhou Z, Liu YG, Liu SB, Liu HY, Zeng GM, Tan XF, Yang CP, Ding Y, Yan ZL, Cai XX (2017) Sorption performance and mechanisms of arsenic(V) removal by magnetic gelatin-modified biochar. Chem Eng J 314:223–231. https://doi.org/10.1016/j.cej.2016.12.113

Zhou H, Zhu W, Yang WT, Gu JF, Gao ZX, Chen LW, Du WQ, Zhang P, Peng PQ, Liao BH (2018) Cadmium uptake, accumulation, and remobilization in iron plaque and rice tissues at different growth stages. Ecotoxicol Environ Saf 152:91–97. https://doi.org/10.1016/j.ecoenv.2018.01.031

Zhou GP, Cao WD, Bai JS, Xu CX, Zeng NH, Gao SJ, Rees RM, Dou FG (2020a) Co-incorporation of rice straw and leguminous green manure can increase soil available nitrogen (N) and reduce carbon and N losses: an incubation study. Pedosphere 30(5):661–670. https://doi.org/10.1016/s1002-0160(19)60845-3

Zhou G, Gao S, Chang D, Rees RM, Cao W (2020b) Using milk vetch (Astragalus sinicus L.) to promote rice straw decomposition by regulating enzyme activity and bacterial community. Bioresour Technol 319:124215. https://doi.org/10.1016/j.biortech.2020.124215

Zhou G, Gao S, Lu Y, Liao Y, Nie J, Cao W (2020c) Co-incorporation of green manure and rice straw improves rice production, soil chemical, biochemical and microbiological properties in a typical paddy field in southern China. Soil till Res 197:104499. https://doi.org/10.1016/j.still.2019.104499

Zhou G, Fan K, Li G, Gao S, Chang D, Liang T, Li S, Liang H, Zhang J, Che Z, Cao W (2023) Synergistic effects of diazotrophs and arbuscular mycorrhizal fungi on soil biological nitrogen fixation after three decades of fertilization. iMeta. https://doi.org/10.1002/imt2.81

Zhu S, Zhao J, Zhao N, Yang X, Chen C, Shang J (2020) Goethite modified biochar as a multifunctional amendment for cationic Cd(II), anionic As(III), roxarsone, and phosphorus in soil and water. J Clean Prod 247:119579. https://doi.org/10.1016/j.jclepro.2019.119579

Zou M, Zhou S, Zhou Y, Jia Z, Guo T, Wang J (2021) Cadmium pollution of soil-rice ecosystems in rice cultivation dominated regions in China: a review. Environ Pollut 280:116965. https://doi.org/10.1016/j.envpol.2021.116965